J. Fluid Mech. (2011), *vol.* 679, *pp.* 122–155.
doi:10.1017/jfm.2011.129

Marine ice sheet dynamics. Part 2. A Stokes flow contact problem

CHRISTIAN SCHOOF†

Department of Earth and Ocean Sciences, University of British Columbia, 6339 Stores Road, Vancouver V6T 1Z4, Canada

(Received 1 January 2009; revised 26 November 2010; accepted 11 March 2011; first published online 17 May 2011)

We develop an asymptotic theory for marine ice sheets from a first-principles Stokes flow contact problem, in which different boundary conditions apply to areas where ice is in contact with bedrock and inviscid sea water, along with suitable inequalities on normal stress and boundary location constraining contact and non-contact zones. Under suitable assumptions about basal slip in the contact areas, the boundary-layer structure for this problem replicates the boundary layers previously identified for marine ice sheets from depth-integrated models and confirms the results of these previous models: the interior of the grounded ice sheet can be modelled as a standard free-surface lubrication flow, while coupling with the membrane-like floating ice shelf leads to two boundary conditions on this lubrication flow model at the contact line. These boundary conditions determine ice thickness and ice flux at the contact line and allow the lubrication flow model with a contact line to be solved as a moving boundary problem. In addition, we find that the continuous transition of vertical velocity from grounded to floating ice requires the presence of two previously unidentified boundary layers. One of these takes the form of a viscous beam, in which a wave-like surface feature leads to a continuous transition in surface slope from grounded to floating ice, while the other provides boundary conditions on this viscous beam at the contact line.

Key words: boundary layers, ice sheets, lubrication theory

1. Introduction

Marine ice sheets are continent-sized ice masses whose base rests on bedrock below sea level. The most important present-day example is the West Antarctic Ice Sheet, estimated to hold enough ice to raise sea levels by 3–5 m. As a result, the dynamics of marine ice sheets has attracted considerable attention over the last five years (e.g. Vieli & Payne 2005; Pattyn *et al.* 2006; Solomon *et al.* 2007; Nowicki & Wingham 2008; Durand *et al.* 2009; Goldberg, Holland & Schoof 2009; Katz & Worster 2010).

From the perspective of fluid dynamics, the grounded portion of a marine ice sheet behaves as gravity-driven, lubrication-type thin-film flow, in which shear stress gradients balance a gravity-induced horizontal pressure gradient. What sets marine ice sheets apart from other examples of such flows (e.g. Balmforth & Craster 1999) is the presence of a contact line at which ice lifts off to form a floating ice shelf.

† Email address for correspondence: cschoof@eos.ubc.ca

The mechanics of the ice shelf is dominated by extensional stresses (or 'longitudinal stresses' in glaciological parlance).

The theoretical challenge in coupling models for shelves and grounded ice sheets is to describe the transition from a shear-stress-dominated to an extensional-stress-dominated flow. In Schoof (2007*b*), henceforth called Part 1, a theory based on matched asymptotic expansions was set out for this transition. This theory predicts that the coupling between grounded sheet and floating shelf leads to two boundary conditions on the diffusion model that describes ice flow in the interior of the grounded ice sheet. One of these boundary conditions fixes ice thickness while the other is a relationship between flux and depth to bedrock at the contact line. Together, these boundary conditions allow the grounded ice sheet flow to be modelled as a Stefan-type free boundary problem.

The consequences of these boundary conditions for the large-scale dynamics of marine ice sheets were explored in Schoof (2007*a*), and the predictions of Part 1 were subsequently confirmed by direct numerical solution of a contact problem for marine ice sheet flow based on the nonlinear Stokes equations that usually underpin ice sheet models (Durand *et al.* 2009).

Despite this numerical confirmation, some theoretical questions remain. In particular, Part 1 was based on a depth-integrated model for the flow of an ice sheet that experiences rapid sliding in its interior. It is desirable to develop an analogous theory that uses a first-principles Stokes flow model and reduces this to the appropriate depth-integrated model, showing that asymptotic matching procedures employed in Part 1 remain valid. In particular, such an approach should answer two questions. Firstly, can the theory in Part 1 be extended to cover ice sheets that experience significant shearing? And secondly, can the transition between grounded and floating ice be captured in more detail than was possible in Part 1?

The second of these points is particularly relevant: the model in Part 1 predicts a discontinuity in vertical velocity at the contact line, which, if real, would require a point force (Wilchinsky & Chugunov 2000). This need not *a priori* represent a serious issue, as the model in Part 1 is depth-integrated and based on a thin-film approximation that may not capture all the details of the transition from grounded to floating ice but can still compute ice flux correctly. There is also every indication that the model in Part 1 is mathematically well-posed, and importantly, the predictions of Part 1 have been confirmed by the direct numerical computations of Durand *et al.* (2009) that are not based on any thin-film approximation. However, it is desirable to understand in detail how the apparent paradox of a vertical velocity discontinuity can be resolved. In fact, we will see later that the apparent point force is simply a vertical force that is spread over a region of the shelf that is small compared with the length scales that are resolved by the depth-integrated model in Part 1. Put another way, the discontinuity in vertical velocity recognized by Wilchinsky & Chugunov (2000) is not an actual discontinuity, but a rapid change in vertical velocity near the grounding line, which is not captured by membrane models and requires consideration of more local physics involved in bending the ice close to the grounding line.

In this paper, we present an asymptotic approach to the type of Stokes flow contact problem solved numerically by Durand *et al.* (2009). The asymptotic structure that we find mimics that found in Part 1, but requires two extra boundary layers that allow a continuous vertical velocity field. These additional boundary layers are passive in the variables modelled in Part 1 (horizontal velocity and ice thickness), and do not affect the validity of the theory developed there. They do, however, resolve the apparent surface slope discontinuity and explain some of the features of the ice sheet surface

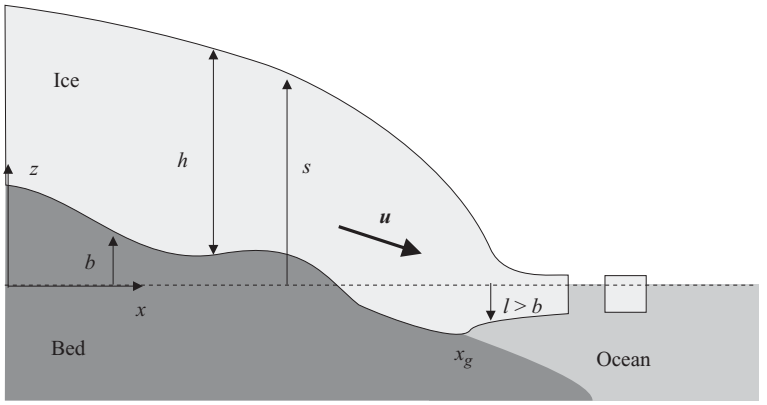

FIGURE 1. Geometry of the problem. Here x and z denote Cartesian coordinates measuring distance in the horizontal and vertical, respectively, $s(x,t)$ is surface elevation above sea level, $h(x,t)$ is ice thickness, $b(x)$ is the elevation of bedrock above sea level (so $b<0$ where bedrock is below sea level) and $l(x,t)$ is the lower boundary of the ice; $l=b$ in contact regions and $l>b$ elsewhere. We assume that there is exactly one contact region which lies upstream of a contact line (or *grounding line*) $x=x_g(t)$ so that $l(x,t)=b(x)$ for $x\leqslant x_g(t)$, while $l(x,t)>b(x)$ for $x>x_g(t)$; $\boldsymbol{u}=(u,v)$ denotes ice velocity.

predicted by Durand *et al.* (2009), most notably an attenuated wave-like surface feature downstream of the contact line, and a non-zero departure from Archimedean flotation at the contact line. Moreover, we find that the theory of Part 1 generalizes straightforwardly to ice sheets that experience shear as well as basal sliding, provided basal sliding becomes dominant near the contact line, and we set out conditions for this to be the case.

To allow an easier presentation of these boundary layers, we do make one simplifying assumption in this paper, to be generalized elsewhere: we restrict ourselves to ice of constant viscosity, with a linear slip law at the base of the ice, while Part 1 and Durand *et al.* (2009) used power laws for both. Using these more restrictive constitutive relations allows us to describe our results in simpler terms, namely by using the intrinsic length scales that are often identified in models of viscous gravity currents (e.g. Lister & Kerr 1989).

2. The model

We model the marine ice sheet as a Newtonian fluid at zero Reynolds number and restrict ourselves to plane flow, with x and z denoting horizontal and vertical positions, respectively, and with z measured upwards from sea level (figure 1). The ice sheet is assumed to be in contact with underlying bedrock at $z=b(x)$ to the left of a moving contact line (or grounding line) at $x=x_g(t)$, and afloat to the right of the contact line (Note that the sign convention for b here is reversed from Part 1, where b denotes bedrock depth *below* sea level). Denoting the lower boundary of the ice by $z=l(x,t)$, this implies $l(x,t)=b(x)$ for $x\leqslant x_g(t)$, and $l(x,t)>b(x)$ for $x>x_g(t)$. The lower boundary of the ice makes contact with the bed at $x=x_g$, so l continuous there. We also use $s(x,t)$ to denote ice surface elevation and $h=s-l$ for ice thickness, while $\boldsymbol{u}=(u,v)$ is ice velocity and p is pressure.

Writing the deviatoric stress tensor in the form

$$\boldsymbol{\tau} = \begin{pmatrix} \tau_1 & \tau_2 \\ \tau_2 & -\tau_1 \end{pmatrix}, \tag{2.1}$$

force balance and conservation of mass in the fluid domain, $l < z < s$, require

$$\tau_{1,x} + \tau_{2,z} - p_x = 0, \tag{2.2a}$$

$$-\tau_{1,z} + \tau_{2,x} - p_z - \rho g = 0, \tag{2.2b}$$

$$u_x + v_z = 0, \tag{2.2c}$$

where ρ is the density of ice, g is acceleration due to gravity, and subscripts x and z denote partial derivatives, so $u_x = \partial u/\partial x$ and $\tau_{1,x} = \partial \tau_1/\partial x$ etc. Stress and strain rate are related through

$$u_x = \frac{1}{2\eta}\tau_1, \tag{2.2d}$$

$$u_z + v_x = \frac{1}{\eta}\tau_2, \tag{2.2e}$$

where the parameter η is viscosity.

At the upper surface, $z = s$, there is no applied traction, which can be written in the form

$$(p - \tau_1)\, s_x + \tau_2 = 0, \tag{2.3a}$$

$$-p - \tau_1 - \tau_2 s_x = 0. \tag{2.3b}$$

In addition, the upper surface evolves according to a kinematic boundary condition with a source term a that describes snowfall or melting (also known as the *accumulation rate*):

$$s_t + u s_x = v + a. \tag{2.3c}$$

At the base of the ice, we need to distinguish between areas of bed contact and non-contact areas. Downstream of the contact line, the base of the ice is in contact with ocean water at a height $z = l(x, t)$ above sea level (i.e. at depth $-l(x, t)$ below sea level). If ρ_w is the density of sea water, the pressure at this depth is $p_w = -\rho_w g l$. Assuming that sea water is inviscid, we get $(p - p_w)\boldsymbol{n} - \boldsymbol{\tau}\boldsymbol{n} = \boldsymbol{0}$, where $\boldsymbol{n} = (-l_x, 1)/\sqrt{1 + l_x^2}$ is the upward-pointing normal to the boundary. In addition, the lower boundary satisfies a kinematic boundary condition analogous to (2.3*c*), where we use m_l in place of a to denote the rate of ice melting (or accretion if $m_l < 0$). We also require that the base of the ice in the non-contact area must remain above bedrock, and so obtain the following conditions for $z = l(x, t)$, $x > x_g(t)$:

$$(p + \rho_w g l - \tau_1) l_x + \tau_2 = 0, \tag{2.4a}$$

$$-p - \rho_w g l - \tau_1 - \tau_2 l_x = 0, \tag{2.4b}$$

$$l_t + u l_x = v + m_l, \tag{2.4c}$$

$$l > b. \tag{2.4d}$$

In general, the ice will have a finite extent, with an ice front at some location $x = x_c(t)$. For simplicity, we assume here that the ice shelf pinches out there with $l = s = 0$. More generally, one would expect a *calving front* to form with a finite ice thickness h, at which icebergs break off.

Upstream of the contact line, the base of the ice is at a fixed elevation $z = b(x)$. We assume zero normal velocity at the bed (no melting or freezing). We also assume

that the ice sheet can slide over the underlying bedrock, and impose a linear slip law. Defining $\boldsymbol{n} = (-b_x, 1)/\sqrt{1+b_x^2}$ and $\boldsymbol{t} = (1, b_x)/\sqrt{1+b_x^2}$ as the upward-pointing normal and tangent to the bed, respectively, sliding velocity $u_t = \boldsymbol{u}\cdot\boldsymbol{t}$ and basal shear stress $\tau_{nt} = \boldsymbol{n}\cdot\boldsymbol{\tau}\boldsymbol{t}$ then satisfy $\tau_{nt} = Cu_t$, where $C > 0$ is constant. (Note that this is the simplest conceivable friction law, and there are many others in the literature, for instance those that include a dependence on subglacial water pressure, see e.g. Lliboutry 1968.) In addition, we impose the following condition for contact with the bed: the normal stress $p - \boldsymbol{n}\cdot\boldsymbol{\tau}\boldsymbol{n}$ must attain or exceed the pressure $-\rho_w g b$ that sea water would exert on the ice at the same elevation, reflecting the fact that water would force its way between ice and bed if this were not the case. Hence, we have on $z = b(x)$, $x < x_g(t)$

$$v = ub_x, \tag{2.5a}$$

$$\frac{-2b_x\tau_1 + (1-b_x^2)\tau_2}{1+b_x^2} = C\left(1+b_x^2\right)^{1/2} u, \tag{2.5b}$$

$$p + \frac{\tau_1\left(1-b_x^2\right) + 2b_x\tau_2}{1+b_x^2} \geqslant -\rho_w g b. \tag{2.5c}$$

Strictly speaking, one could allow the possibility that a part of the ice surface in contact with the bed is just about to be lifted off (see also Durand *et al.* 2009). In that case, the conditions (2.5) have to be replaced on those areas with (2.4), but with $l = b$ instead of (2.4*d*) and (as the ice is lifting off) the additional constraint $v > ub_x$. However, such regions cannot persist for finite time intervals (as these conditions lead to $l > b$ after any finite time), and for this reason we ignore them here.

The significance of the contact inequalities (2.4*d*) and (2.5*c*) will be discussed in much greater detail in a separate paper concerned solely with flow in the vicinity of the contact line (C. Schoof, 2011, in preparation). Here we remark simply that they are essential in determining implicitly the position of the contact line $x_g(t)$ as the ice sheet evolves. Without these inequalities, there is apparently nothing to stop us from fixing the location of x_g arbitrarily and still satisfying the equalities in (2.4) and (2.5). This point is illustrated by the numerical computations of ice flow near a grounding line in Nowicki & Wingham (2008) and Durand *et al.* (2009), while a similar situation is encountered in the study of cavitation at the base of a Stokes flow in Schoof (2005) and Gagliardini *et al.* (2007). Similar inequalities also occur in elastic Signorini-type contact problems (Kikuchi & Oden 1988).

3. A sketch of the flow structure of the marine ice sheet

To motivate the more detailed work below, we sketch the essential features of the flow here using a number of simplifying assumptions that we will either justify or dispense with in the analysis in §4 (I am indebted to one of the referees for suggesting this presentation). The advantage of the simpler treatment given here is that it motivates many of the scalings used later. Note that the treatment below is constructive rather than deductive in the sense that we seek to construct *a* viable solution to the marine ice sheet problem (and to identify any limitations on its validity) rather than to explore all the possible flow structures that could arise from all possible parameter choices. (An attempt at a deductive approach may be found in Wilchinsky & Chugunov 2001.) We also give forward references in the sketch here to the corresponding part of the analysis in §4.

Consider the grounded part of the ice sheet, where $x < x_g$. Assume that this has a low aspect ratio and that extensional stresses are small. Then ice flux is the sum of a Poiseuille-like contribution due to shearing and a contribution due to slip (§ 4.2). For a nearly flat bed (so $s_x \approx h_x$),

$$q = -\frac{\rho g}{\eta}\left(\frac{h^3}{3} + L_s h^2\right) h_x, \tag{3.1}$$

where we define a slip length scale

$$L_s = \eta / C. \tag{3.2}$$

Physically, L_s is a thickness scale at which slip and shear contribute comparably to flux.

Now suppose that the ice sheet is in steady state with zero inflow at $x = 0$, in which case

$$q(x) = \int_0^x a(x')\,\mathrm{d}x' \tag{3.3}$$

is a known function. Assume for simplicity that a is concentrated near $x = 0$, so that q can be treated as constant for most of the domain. Integration of (3.1) then yields

$$\frac{\rho g}{\eta}\left(\frac{h^4}{12} + \frac{L_s h^3}{3}\right) = q(x_0 - x), \tag{3.4}$$

where x_0 is a constant of integration that we will identify shortly with the approximate location of the contact line. Rearranging,

$$\frac{1}{12}h^4 + \frac{1}{3}L_s h^3 = \frac{q\eta}{\rho g}(x_0 - x) = L_q^3(x_0 - x), \tag{3.5}$$

where

$$L_q = \left(\frac{\eta q}{\rho g}\right)^{1/3} \tag{3.6}$$

is a viscous length scale (Lister & Kerr 1989). (Physically, L_q is the thickness scale at which an $O(1)$ surface slope will generate a flux q through shearing. This situation is never realized in the present case, but nevertheless L_q remains a useful intrinsic length scale to work with.)

From (3.1) we have a flow that is dominated by shearing if $h \gg L_s$, and from (3.5), this is the case if $x_0 - x \gg L_q(L_s/L_q)^4$. The flow is dominated by slip if $h \ll L_s$, corresponding to $x_0 - x \ll L_q(L_s/L_q)^4$, with both slip and shearing contributing comparably when $h \sim L_s$, $x_0 - x \sim L_q(L_s/L_q)^4$ (figure 2).

We can also check *a posteriori* that extensional stress gradients are small and that the aspect ratio is small, which are the prerequisites for (3.1) to apply. Small surface slopes $h_x \ll 1$ (and hence the assumption of a small aspect ratio) are self-consistent with the solution (3.5) so long as $x_0 - x \gg L_q(L_q/L_s)^{1/2}$. Extensional stresses are greatest in the slip-dominated region, where we have $u \sim -(\rho g L_s/\eta)hh_x$ and so extensional stress behaves as

$$\tau_1 = 2\eta u_x \sim -\rho g L_s (h^2)_{xx} \sim \frac{2\rho g L_s^{2/3} L_q^2 (x_0 - x)^{-4/3}}{3^{4/3}}, \tag{3.7}$$

where we have also used (3.5) in the slip-dominated regime, where $h \sim L_q[3(x_0 - x)/L_s]^{1/3}$. In order for (3.1) and therefore (3.5) to apply, the extensional stress gradient

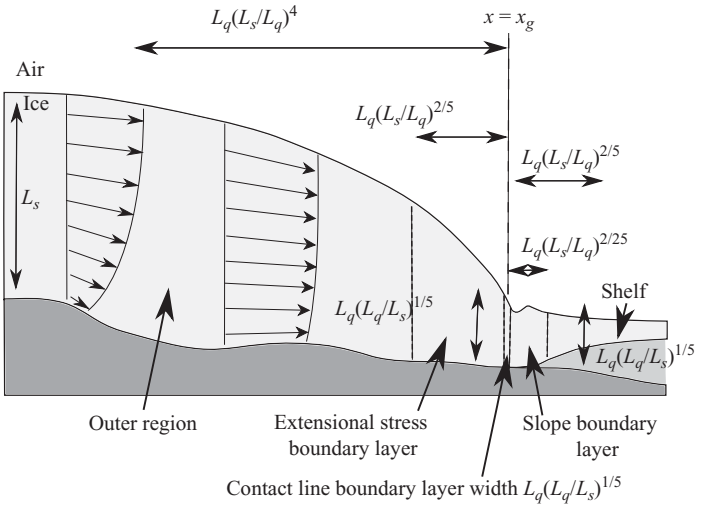

FIGURE 2. An illustration of some of the length scales that arise in the problem (vertically exaggerated). Also shown are typical velocity profiles. Note that sliding and shearing are of comparable magnitude when $x_g - x \sim L_q(L_s/L_q)^4$, but sliding starts to dominate when $x_g - x \ll L_q(L_s/L_q)^4$. Extensional stresses become important when $x_g - x \sim L_q(L_s/L_q)^{2/5}$.

$\tau_{1,x}$ must be small compared with the pressure gradient $\rho g h_x$ driving the flow. This is the case when

$$x_0 - x \gg L_q^{3/5} L_s^{2/5}. \tag{3.8}$$

From (3.5), we therefore see that extensional stresses are small where $h \gg L_q^{6/5} L_s^{-1/5}$, or conversely, become important when $h \sim L_q^{6/5} L_s^{-1/5}$ (§ 4.3).

Provided that $L_s \gg L_q$, we can therefore identify three different regions. One has $x_0 - x \gg L_q(L_s/L_q)^4$ and $h \gg L_s$, and flow is dominated by shearing. When $L_q(L_s/L_q)^4 \gg x_0 - x \gg L_q^{3/5} L_s^{2/3}$, we have $L_q^{6/5} L_s^{-1/5} \ll h \ll L_s$ and a flow dominated by slip, but extensional stresses and surface slopes remain small, with an overlap region between shear- and slip-dominated regimes when $x_0 - x \sim L_q(L_s/L_q)^4$ and $h \sim L_s$. Finally, when $x_0 - x \sim L_q^{3/5} L_s^{2/5}$ and $h \sim L_q^{6/5} L_s^{-1/5}$, the assumption of negligible extensional stresses in (3.1) breaks down, but surface slopes are still small as $x_0 - x \gg L_q$, and a viscous membrane model is required. Note that this separation of scales only requires $L_s \gg L_q$; this is the parameter regime we assume in this paper.

Whether all four of these regions exist depends on the horizontal extent L of the ice sheet. We will also assume that we have at least $L \gg L_q^{3/5} L_s^{2/5}$, so that at least one of the regions in which extensional stresses are small exists.

In the region where $x_0 - x \sim L_q^{3/5} L_s^{2/5}$ and $h \sim L_q^{6/5} L_s^{-1/5}$, the lubrication flow model (3.1) no longer holds, as extensional stresses feature at leading order in force balance (§ 4.3). We have a viscous membrane-like model (Erneux & Davis 1993; Oron, Davis & Bankoff 1997)

$$4(\eta h u_x)_x - \eta u / L_s - \rho g h h_x = 0, \quad uh = q, \tag{3.9}$$

which matches to (3.1) in a matching region where $L_q(L_s/L_q)^4 \gg x_0 - x \gg L_q^{3/5} L_s^{2/5}$ (§ 4.4).

Ice thickness progressively becomes smaller as we pass from the shear-dominated to the slip-dominated region and finally onto the extensional-stress-influenced region

$x_0 - x \sim L_q^{3/5} L_s^{2/5}$. Ice thickness does however not pinch out in the grounded part of the ice sheet. Instead, ice reaches the contact line $x = x_g$ (with $x_0 - x_g \sim L_q^{3/5} L_s^{2/5}$), where it begins to float and an ice shelf is attached to the ice sheet. From the contact inequalities (2.4*d*) and (2.5*c*) and an approximately 'cryostatic' normal stress $p + \tau_1$, the thickness at the contact line can be approximated as the critical thickness at which ice begins to float in the Archimedean sense (§ 4.6), so

$$h(x_g) = -\rho_w b(x_g)/\rho. \tag{3.10}$$

The shelf itself satisfies a viscous membrane model (§ 4.5) similar to (3.9) above and to the 'free film' in e.g. Erneux & Davis (1993),

$$4(\eta h u_x)_x - \rho(1 - \rho_/\rho_w) g h h_x = 0, \quad uh = q. \tag{3.11}$$

The first of these equations integrates to

$$2\eta h u_x = \rho((1 - \rho/\rho_w) g h^2/4, \tag{3.12}$$

and the shelf therefore exerts an extensional stress

$$2\eta h u_x|_{x=x_g} = \rho(1 - \rho/\rho_w) g h(x_g)/4 = -\rho_w(1 - \rho/\rho_w) g b(x_g)/4 \tag{3.13}$$

on the grounded ice at the contact line (§ 4.6).

This integration of (3.11) allows us to close the problem (3.9) using (3.10) and (3.13) and matching with the lubrication-type flow. In the scenario we consider above, q is prescribed, and the boundary-layer problem (3.9) in fact allows us to compute $b(x_g)$ from the given value of q (the Appendix), and this implicitly locates the contact line x_g in the steady-state case considered here. In a dynamic model, the boundary-layer problem instead provides a relationship between $b(x_g)$ and q at the grounding line, which then becomes a boundary condition on the non-steady equivalent of (3.3), which takes the form of a diffusion equation for h.

We are in particular interested in the case where x_g is a free boundary whose location can vary over the entire length L of the ice sheet as accumulation rate a and hence ice flux q is varied, rather than having the contact line confined to a sharp drop-off in the bed of the ice sheet. (This is the dynamically most interesting case of a marine ice sheet, and is relevant to the present-day West Antarctic Ice Sheet.) The sketch above indicates that this is most easily accommodated if the shelf joins the region where extensional stress is significant, where ice thickness is $\sim L_q^{6/5} L_s^{-1/5}$ (which is small compared with ice thickness in the interior of the ice sheet).

But from (3.10), this indicates that bedrock depth $-b$ below sea level must therefore also scale with $L_q^{6/5} L_s^{-1/5}$, which we will assume to be the case in the manner of a distinguished limit (§ 4.1; this echoes a similar result in Part 1, where depth to bedrock also had to be small if a balance between mass accumulation $\int_0^{x_g} a \, \mathrm{d}x$ and outflow into the shelf was to be assumed).

The coupling between (3.9) and (3.11) sketched above was achieved by simply enforcing continuity of velocity, thickness and stress (§ 4.6). However, enforcing these continuity requirements runs into one problem, namely that the base of the boundary layer region of the grounded sheet is controlled by bed topography, and is nearly flat, while the base of the shelf is controlled by the requirement that the shelf be afloat and by the downstream thinning rate of the membrane-like shelf. This engenders an apparent discontinuity in the slope at the base of the ice and hence in vertical velocity. Such a discontinuity cannot exist in reality, as it would require a point force (Wilchinsky & Chugunov 2000, 2001). A continuous transition is instead ensured by

a short part of the shelf that acts as a viscous beam (§ 4.7), and essentially spreads out Wilchinsky–Chugunov's point force over a small but finite region ('small' meaning short by comparison with the shelf).

If $h_g = -\rho_w b(x_g)/\rho$ is ice thickness at the contact line, then beam theory gives

$$-\frac{\eta h_g^3}{3} v_{l,xxxx} = \rho g \Delta s + \rho_w (1 - \rho/\rho_w) g \Delta l, \tag{3.14}$$

where v_l is vertical velocity at the base of the ice, and Δs and Δl are the deflections of the surface and base of the ice from their Archimedean flotation positions at the contact line, respectively. In steady state, vertical velocity and deflection of the base are linked through a kinematic boundary condition, $v_l = u \Delta l_x$, with a similar equation for Δs, and by differentiating (3.14) and using $u = q/h_g$, we get

$$-\frac{\eta h_g^3}{3} v_{l,xxxxx} = \rho_w g (h_g/q) v_l - \rho g h_x. \tag{3.15}$$

The second term on the right-hand side arises from differentiating Δs and represents the rate at which the shelf thins in the downstream direction, which causes the base of the ice shelf to move up at a mean rate $v_l \sim (\rho/\rho_w) h_x/u$. The fifth-order differential equation (3.15) gives a length scale

$$[\rho g/(q\eta)]^{-1/5} h_g^{2/5} \sim L_q^{3/5} (L_q^{6/5} L_s^{-1/5})^{2/5} = L_q^{27/25} L_s^{-2/25} \tag{3.16}$$

(using $h_g \sim L_q^{6/5} L_s^{-1/5}$, and treating ρ/ρ_w and $(1 - \rho/\rho_w)$ as $O(1)$). For $L_s \gg L_q$, this length scale is much smaller than the horizontal length scale $L_q^{3/5} L_s^{2/5}$, but still longer than the thickness scale $h_g \sim L_q^{6/5} L_s^{-1/5}$, justifying the use of a beam model. The viscous beam bending does not affect extensional stress, thickness or horizontal velocity at leading order, and coupling (3.9) and (3.11) through these continuity conditions remains correct.

The beam model (3.15) applies on the 'floating' side of the contact line, and there is no bending on the grounded side. The transition between beam and the grounded ice requires boundary conditions on the beam equation; specifically, these boundary conditions are that vertical velocity at the bed as well as vertical shear and bending moment in the beam vanish at the contact line. To justify them properly requires an additional boundary layer of horizontal extent equal to ice thickness in which the full Stokes equations must be solved (§ 4.8).

4. An asymptotic analysis of the model

4.1. *Non-dimensionalization*

Our goal in this paper is to use asymptotic methods to derive a simplified free boundary model for the marine ice sheet along the lines of Part 1, showing in detail the role played by the different components of flow structure sketched in the previous section. To this end, we scale the model first and identify the relevant small parameters in which the solution can be expanded.

In the previous section, scales for various boundary layers were derived in terms of the 'intrinsic' length scales L_q and L_s. These boundary layers will ultimately provide boundary conditions for a simplified free boundary problem that describes the evolution of ice thickness and the migration of the contact line. We envisage ice thickness and contact line position to vary over the length scale L of the ice sheet. Here L is therefore an essential length scale for the problem (amongst other things,

L sets a natural time scale for the time-dependent flow problem), even though it is not an intrinsic length scale defined by material properties, unlike L_s and L_q.

In total, we have three length scales, and it is possible to develop an asymptotic solution in terms of the length-scale ratios L_s/L and L_q/L_s. This is so only because we have a Newtonian flow with a linear friction law. Intrinsic length scales are much harder to motivate in the case of the power-law viscosity and friction laws that were used in Part 1. With a view to allowing the work here to be generalized to these power-law constitutive relations, we develop our asymptotic approach instead in terms of an aspect ratio and a stress ratio parameter that we will relate to the ratios L_q/L and L/L_s, but which can also be defined for more general power-law constitutive relations.

Our choice of scales is based on the approach in Schoof & Hindmarsh (2010). We assume that a horizontal length scale $[x] = L$ for the ice sheet is known from the shape of the underlying bedrock, and that the accumulation rate scale $[a]$ is also known. This leaves scales for time $[t]$, thickness $[h]$, velocities $[u]$ and $[v]$ and stresses $[\tau_1]$ and $[\tau_2]$ to be determined. We define these six scales implicitly through the six scale relations

$$[u]\,[h] = [a]\,[x], \tag{4.1a}$$

$$[\tau_2] = \rho g\,[h]^2 / [x]\,, \tag{4.1b}$$

$$C\,[u] = [\tau_2]\,, \tag{4.1c}$$

$$\eta\,[u]\,/[x] = [\tau_1]\,, \tag{4.1d}$$

$$[v]\,/[h] = [u]/[x], \tag{4.1e}$$

$$[t] = [x]/[u]. \tag{4.1f}$$

With velocity $[u]$ defined through (4.1c), these balances are appropriate for a flow in which slip either dominates or is comparable to shear. The model is scaled as follows:

$$\left.\begin{array}{l} h = [h]\,h^*, \quad s = [h]s^*, \quad z = [h]\,z^*, \quad x = [x]\,x^*, \\ t = [t]t^*, \quad a = [a]\,a^*, \quad m_l = [a]\,m_l^*, \\ u = [u]\,u^*, \quad v = [v]\,u^*, \quad \tau_1 = [\tau_1]\,\tau_1^*, \quad \tau_2 = [\tau_2]\,\tau_2^*, \quad p = \rho g\,[h]\,p^*. \end{array}\right\} \tag{4.2}$$

We also define three dimensionless parameters: an aspect ratio ν, a stress ratio ε and a density ratio:

$$\nu = \frac{[h]}{[x]}, \quad \varepsilon = \frac{[h]\,[\tau_1]}{[x]\,[\tau_2]}, \quad r = \frac{\rho}{\rho_w}. \tag{4.3}$$

It will become apparent below that ε is identical to the parameter denoted by the same symbol in Part 1, with the caveat that our constitutive relations here are more restrictive than in Part 1. Note that ν and ε can be related to the length scales L, L_s and L_q. If we take $[x] = L$, $[q] = [u][h] = [a][x]$ and define $L_q = (\eta[q]/\rho g)^{1/3}$, $L_s = \eta/C$, then some algebra yields

$$\nu = \frac{L_q}{L}\left(\frac{L}{L_s}\right)^{1/3}, \quad \varepsilon = \nu\frac{L_s}{L} = \frac{L_q}{L}\left(\frac{L_s}{L}\right)^{2/3}, \tag{4.4}$$

$L_s = (\varepsilon/\nu)L$, $L_q = \nu^{2/3}\varepsilon^{1/3}L$. The sketch in the previous section leads us to consider the case $L_q \ll L_s$ and $L_q^{3/5}L_s^{2/5} \ll L$ and. In terms of ν and ε, these two inequalities read, respectively

$$\nu^{5/2} \ll \varepsilon, \quad \varepsilon \ll 1. \tag{4.5}$$

Taken together, these immediately ensure a small aspect ratio $\nu \ll 1$. In Part 1, where we employed a depth-integrated model from the start, the only explicit requirement was that $\varepsilon \ll 1$, and implicitly (to be able to depth-integrate) $\nu \ll 1$. The above indicates that the constraint on ν is in fact more restrictive: this is necessary to ensure that all the boundary layers sketched in § 3 are scale separated, and importantly, to ensure that the extensional stress boundary layer has a low aspect ratio. For completeness, we note that we treat the density ratio $r \approx 0.9$ as well as $1 - r \approx 0.1$ as $O(1)$ parameters. This is entirely self-consistent and only requires that ε and hence ν are sufficiently small for the relevant asymptotic limits to apply. The limit of small $1 - r$ is clearly also of interest as this quantity, though of fixed value for given materials, is numerically small. Part 1 indicates that an alternative theory is required when $\varepsilon \sim (1 - r) \ll 1$; due to space constraints, we defer discussion of this limit to future work.

In view of the discussion in § 3, we anticipate that a leading-order model in which the contact line can migrate over distances $\sim L$ will only arise if bed topography is sufficiently small everywhere (comparable to ice thickness in the extensional stress boundary layer). The relevant scale is $[b] = L_q^{6/5} L_s^{-1/5}$, which after some algebra turns out to be $[b] = \varepsilon^{1/5}[h]$, and we define

$$b = [b]b^*, \quad l = [b]l^*. \tag{4.6}$$

In what follows, we will treat b^* as a prescribed, $O(1)$ function of the variable x^*, assuming that it changes by amounts of $O(1)$ only when x^* changes by $O(1)$, so that we can treat its derivative $b^*_{x^*}$ as being of $O(1)$, too. This is a somewhat restrictive assumption on bed topography that we discuss further in § 6; we note however that the above is analogous to the scaling of bedrock in § 3.3 of Part 1.

For simplicity, we immediately drop the asterisks on scaled variables. In scaled form, the model (2.2)–(2.5) becomes the following. In $\varepsilon^{1/5} b < z < s$,

$$\varepsilon \tau_{1,x} + \tau_{2,z} - p_x = 0, \tag{4.7a}$$

$$-\varepsilon \tau_{1,z} + \nu^2 \tau_{2,x} - p_z - 1 = 0, \tag{4.7b}$$

$$u_x + v_z = 0, \tag{4.7c}$$

$$2u_x = \tau_1, \tag{4.7d}$$

$$u_z + \nu^2 v_x = \nu^2 \varepsilon^{-1} \tau_2. \tag{4.7e}$$

Boundary conditions at the upper surface $z = s = h + \varepsilon^{1/5} b$ are

$$(p - \varepsilon \tau_1) s_x + \tau_2 = 0, \tag{4.8a}$$

$$-p - \frac{\nu}{\lambda} \tau_1 - \nu^2 \tau_2 s_x = 0, \tag{4.8b}$$

$$s_t + u s_x = v + a. \tag{4.8c}$$

On the non-contact parts of the base of the ice, $z = \varepsilon^{1/5} l$, $x > x_g$, we have

$$\varepsilon^{1/5} \left(p + \varepsilon^{1/5} r^{-1} l - \varepsilon \tau_1 \right) l_x + \tau_2 = 0, \tag{4.9a}$$

$$-p - \varepsilon^{1/5} r^{-1} l - \varepsilon \tau_1 - \nu^2 \varepsilon^{1/5} \tau_2 l_x = 0, \tag{4.9b}$$

$$\varepsilon^{1/5} (l_t + u l_x) = v + m_l, \tag{4.9c}$$

$$l > b, \tag{4.9d}$$

while for the contact areas $z = \varepsilon^{1/5} b$, $x < x_g$,

$$v = \varepsilon^{1/5} u b_x, \tag{4.10a}$$

$$\frac{-2\varepsilon^{6/5} b_x \tau_1 + (1 - \nu^2 \varepsilon^{2/5} b_x^2)\tau_2}{1 + \nu^2 \varepsilon^{2/5} b_x^2} = \left(1 + \nu^2 \varepsilon^{2/5} b_x^2\right)^{1/2} u, \tag{4.10b}$$

$$p + \frac{\varepsilon(1 - \nu^2 \varepsilon^{2/5} b_x^2)\tau_1 + 2\nu^2 \varepsilon^{1/5} b_x \tau_2}{1 + \nu^2 \varepsilon^{2/5} b_x^2} \geqslant -\varepsilon^{1/5} r^{-1} b. \tag{4.10c}$$

Note that the complicated powers of ε appear in these boundary conditions due to our choice of scales for b above.

4.2. *Grounded ice sheet flow: the outer problem*

The grounded ice flow in the interior of the ice sheet ($0 < x_g - x = \mathrm{Ord}(1)$) is the outer problem for which the scalings chosen above are appropriate. By insisting that ν and ε are small, we can omit terms of $O(\nu)$, $O(\varepsilon)$ and hence of $O(\varepsilon^{1/5})$ in (4.7), (4.8) and (4.10) to find

$$\tau_{2,z} - p_x = 0, \quad p_z = -1, \quad u_x + v_z = 0, \quad u_z = \nu^2 \varepsilon^{-1} \tau_2 \tag{4.11a}$$

in the interior of the ice, which is $0 < z < s$ at leading order, with $s = h$ at leading order. Boundary conditions are

$$\tau_2 = 0, \quad p = 0, \quad s_t + u s_x = v + a \tag{4.11b}$$

on $z = s$, and

$$\tau_2 = u, \quad v = 0, \quad p \geqslant O(\varepsilon^{1/5}) \tag{4.11c}$$

on $z = 0$. In the last equality in (4.11a), we have retained the $O(\nu^2\varepsilon^{-1})$ shearing term on the right-hand side as a leading-order contribution. This is apparently appropriate only when $\nu^2\varepsilon^{-1} \lesssim 1$, or equivalently, when $L_q L^{1/3}/L_s^{4/3} \lesssim 1$ and so $L \lesssim L_s^4/L_q^3$. But reference to § 3 shows that this is nothing more than the restriction that the ice sheet not be large enough for the shear-dominated regime to appear. A flow in which sliding is at least as important as shearing is also suggested out by the choice of scale $[u]$ in (4.1). For the sake of brevity, we assume that this is the case. It should be clear, however, that it is possible to add the shear-dominated regime through a rescaling and that the same thin film model as we are about to derive also captures the shear-dominated regime; we merely chose not to expend journal space on the relevant rescaling that would formally describe the shear-dominated regime.

The outer problem can be solved for velocity and stress as

$$p = s - z, \quad \tau_2 = -(s - z) s_x, \tag{4.12}$$

$$u = -s s_x - \frac{\nu^2}{2\varepsilon}\left[s^2 - (s - z)^2\right] s_x, \tag{4.13}$$

where the $O(\nu^2\varepsilon^{-1})$ shearing term could once again be omitted if $\nu^2 \ll \varepsilon$. From $(4.11a)_3$, $(4.11b)_3$ and $(4.11c)_2$, surface evolution is described through the depth-integrated mass conservation equation

$$s_t + q_x = a, \quad q = \int_0^s u \, \mathrm{d}z. \tag{4.14}$$

Using the form of u in (4.13), we find

$$q = -\left[s^2 s_x + \frac{\nu^2}{3\varepsilon} s^3 s_x\right], \tag{4.15}$$

which we can identify as the scaled form of (3.1). Therefore

$$s_t - \left[s^2 s_x + \frac{\nu^2}{3\varepsilon} s^3 s_x \right]_x = a. \tag{4.16}$$

In addition to the diffusion problem (4.16), we have from the inequality in (4.11*c*) the trivial requirement that

$$s > 0. \tag{4.17}$$

In other words, ice thickness $h \sim s$ must not go to zero in the outer region in order satisfy the contact inequality.

Before we consider what happens closer to the contact line, we should make the link with Part 1 clearer, as our boundary-layer problem will turn out to be a special case of that considered in Part 1. The model used in Part 1, with the rheological coefficients m and n set to unity, can be obtained from (4.7)–(4.10) if we take only the asymptotic limit $\nu \ll 1$ and allow ε initially to be of $O(1)$. In that case, it is easy to show that we obtain from dropping terms of $O(\nu)$ and a series of simple quadratures that $u \sim u(x,t)$ is independent of z and we get the following 'free film with friction' (Erneux & Davis 1993) or 'ice stream' model (Muszynski & Birchfield 1987; MacAyeal 1989; Schoof & Hindmarsh 2010):

$$4\varepsilon(hu_x) - u - (h - \varepsilon^{1/5} b)s_x = 0, \quad h_t + (uh)_x = a, \tag{4.18}$$

which is of the same form as that studied in Part 1, with ε denoting the same dimensionless parameter. (To see how this series of quadratures works, see either the Appendix of Schoof (2006) or the procedure in § 4.3 below). Subsequent use of $\varepsilon^2 \ll 1$ retrieves (4.15) with the $O(\nu^2/\varepsilon)$ shearing term omitted.

4.3. *The extensional stress boundary layer*

This boundary layer is the part of the grounded ice sheet in which extensional stresses begin to be important. The sketch of the flow structure in § 3 suggests that the boundary layer length scale is $L_q^{3/5} L_s^{2/5} = \varepsilon^{3/5} L$, where ice thickness scales as $L_q^{6/5} L_s^{-1/5} = \varepsilon^{1/5}[h] = [b]$. We expect dimensionless flux to remain $O(1)$ in the boundary layer, which suggests the rescaling

$$x - x_g = \varepsilon^{3/5} X, \quad h = \varepsilon^{1/5} H, \quad u = \varepsilon^{-1/5} U. \tag{4.19}$$

Note that these rescalings agree with those for the normal stress boundary layer in Part 1 for the parameter choice $m = n = 1$ appropriate for the linear slip law and Newtonian rheology considered here. We also require additional rescalings for the remaining variables:

$$z = \varepsilon^{1/5} Z, \quad s = \varepsilon^{1/5} S \quad \tau_1 = \varepsilon^{-4/5} T_1, \quad \tau_2 = \varepsilon^{-1/5} T_2, \quad v = \varepsilon^{-3/5} V, \quad p = \varepsilon^{1/5} P. \tag{4.20}$$

To simplify our notation, we define an aspect ratio ν' for the boundary layer as

$$\nu' = \nu \varepsilon^{-2/5} = \left(\frac{L_q}{L_s} \right)^{3/5}. \tag{4.21}$$

Equations (4.7), (4.8) and (4.10) can now be written in terms of the rescaled variables as

$$T_{1,X} + T_{2,Z} - P_X = 0, \tag{4.22a}$$

$$-T_{1,Z} + \nu'^2 T_{2,X} - P_Z = 0, \tag{4.22b}$$

$$U_X + V_Z = 0, \tag{4.22c}$$

$$2U_X = T_1, \tag{4.22d}$$

$$U_Z + \nu'^2 V_X = T_2, \tag{4.22e}$$

on $b(x_g + \varepsilon^{3/5}X) < Z < S$, with

$$(P - T_1)S_X + T_2 = 0, \tag{4.23a}$$

$$-P - T_1 - \nu'^2 T_2 S_X = 0, \tag{4.23b}$$

$$\varepsilon^{4/5}S_t - \varepsilon^{1/5}\dot{x}_g S_X + U S_X = V + \varepsilon^{4/5}a, \tag{4.23c}$$

on $Z = S$, where $\dot{x}_g = \mathrm{d}x_g/\mathrm{d}t$, and

$$\frac{-2\varepsilon^{3/5}b_x T_1 + \left(1 - \nu'^2\varepsilon^{6/5}\right)b_x^2 T_2}{1 + \nu'^2\varepsilon^{6/5}b_x^2} = \left(1 + \nu'^2\varepsilon^{6/5}b_x^2\right)^{1/2} U, \tag{4.24a}$$

$$V = \varepsilon^{3/5} U b_x, \tag{4.24b}$$

$$P + \frac{\left(1 - \nu'^2\varepsilon^{6/5}b_x^2\right)T_1 + 2\nu'^2\varepsilon^{3/5}b_x T_2}{1 + \nu'^2\varepsilon^{6/5}b_x^2} \geqslant -r^{-1}b, \tag{4.24c}$$

on $Z = b(x_g + \varepsilon^{3/5}X)$, $X < 0$.

These equations simplify if the boundary layer can be treated as having a small aspect ratio ν', or equally, if $\nu^{5/2} \ll \varepsilon$ as imposed in (4.5). In terms of the intrinsic length scales L_q and L_s, the statement $\nu^{5/2} \ll \varepsilon$ is equivalent to $L_s \gg L_q$, which was the basis for the separation of scales in § 3.

Note also that we assume that b changes significantly over length scales comparable with the ice sheet size L. Consequently, in the boundary layer, we will treat $b(x_g + \varepsilon^{3/5}X) \sim b(x_g)$ as constant at leading order. With these assumptions, the problem above can be simplified to

$$T_{1,X} + T_{2,Z} - P_X = 0, \tag{4.25a}$$

$$-T_{1,Z} - P_Z - 1 = 0, \tag{4.25b}$$

$$U_X + V_Z = 0, \tag{4.25c}$$

$$T_1 = 2U_X, \tag{4.25d}$$

$$U_Z = 0 \tag{4.25e}$$

on $b(x_g) < Z < S$, with

$$(P - T_1)S_x + T_2 = 0, \quad P + T_1 = 0, \quad U S_X = V \tag{4.26}$$

on $Z = S$, and

$$V = 0, \quad T_2 = U, \quad P + T_1 \geqslant -r^{-1}b(x_g) \tag{4.27}$$

on $Z = b(x_g)$, all of the above being valid in the contact region, where $X < 0$.

From (4.25b) and (4.26)$_2$, we find $P + T_1 = S - Z$. Moreover, from (4.25e), $U = U(X, t)$ is independent of Z (the boundary layer is a plug flow) and from (4.25d), $T_1 = 2U_X$ is also independent of Z. Substituting $P = S - Z - T_1$ in (4.25a) gives

$$2T_{1,X} + T_{2,Z} - S_X = 0. \tag{4.28}$$

Integrating this from $Z = b(x_g)$ to $Z = S$, using the boundary conditions $(4.26)_1$, (4.27) as well as (4.25*d*) and noting that to leading order b is independent of the inner coordinate X, we find

$$4(HU_X)_X - U - HH_X = 0, \tag{4.29a}$$

where $H = S - b(x_g)$ is ice thickness. Meanwhile, integrating (4.25*c*) from $Z = b(x_g)$ to $Z = S$ and using $(4.26)_3$ and $(4.27)_2$ yields

$$(UH)_X = 0. \tag{4.29b}$$

Meanwhile, the contact inequality $(4.27)_3$ becomes

$$H \geqslant -r^{-1}b(x_g), \tag{4.29c}$$

with (4.29*a*)–(4.29*c*) in the contact region $X < 0$. For $X > 0$, we have boundary conditions at the base of the ice that correspond to contact with sea water, which require separate treatment in §§ 4.5–4.7.

In (4.29*a*)–(4.29*c*), we have the same boundary layer problem as in Part 1 (equation (3.39) of Part 1 with $m = n = 1$). We still need to find appropriate boundary conditions for this boundary layer problem.

4.4. *Matching with the outer problem*

The outer and boundary layer solutions must match in a matching region where $x_g - x \ll 1$ and $X \gg 1$. By (4.29*b*), ice flux UH is constant in the boundary layer, and we denote this by $Q = UH$, so $U = Q/H$. In the matching region, we expect

$$q \sim Q, \quad u \sim \varepsilon^{-1/5}U, \quad h \sim \varepsilon^{1/5}H, \tag{4.30}$$

where q and u are given by (4.13) and (4.15) and U and H are solutions of (4.29). Rewriting (4.13) in terms of the boundary layer variables S, Z and X gives

$$u = -\varepsilon^{-1/5}\left\{SS_X + \frac{\nu^2}{2\varepsilon^{4/5}}\left[S^2 - (S-Z)^2\right]S_X\right\}. \tag{4.31}$$

From (4.30) with $U = U(X, t)$ independent of Z, we see that matching requires the second term in curly brackets in (4.31) to be small at leading order. In other words, the outer velocity field must turn into a plug flow in the matching region. This is the case when the coefficient $\nu^2/\varepsilon^{4/5} = \nu'^2$ is small, that is, precisely when $(4.5)_1$ is satisfied. Under these circumstances, we have

$$u \sim -\varepsilon^{1/5}SS_X \sim -\varepsilon^{1/5}U, \tag{4.32}$$

which corresponds to (4.29*a*) in the limit of $U_X \to 0$, $H \to \infty$ (where $H \sim S$). From this and (4.30), we can therefore identify the relevant matching conditions at leading order as

$$U \to 0, \quad U \sim -HH_X, \quad \text{as } X \to -\infty, \tag{4.33a}$$

$$h \to 0, \quad q \to Q, \quad \text{as } x \to x_g^-, \tag{4.33b}$$

$x \to x_g^-$ denoting the limit taken as $x_g(t)$ is approached from below. Note that $h \to 0$ and $q = -hh_x \to Q$ as x approaches x_g from below together imply that $Q > 0$.

As in Part 1, we see again that matching with the normal stress boundary layer supplies the required two boundary equations for the diffusion problem (4.16) at the moving boundary $x = x_g(t)$ through (4.33*b*), one on ice thickness h (or equivalently, on surface elevation $s \sim h$ in the outer region) and the other on ice flux q. To close the outer problem, the flux Q must still be found, which requires the boundary-layer

problem (4.29) to be solved. To this end, we still need boundary conditions for (4.29) at the grounding line $X = 0$. These arise from coupling the normal stress boundary layer with the ice shelf, which we consider next.

4.5. *The ice shelf*

The rescalings for stress, velocity and ice thickness in the normal stress boundary layer were chosen to allow the lubrication flow in the interior of the ice sheet to be coupled to the ice shelf. If the normal stress boundary layer does couple straightforwardly to the shelf, then it is natural to expect the same rescalings to apply to the shelf itself. In addition to (4.19), we define

$$l(x,t) = L(X,t), \quad m_l = \varepsilon^{3/5} M. \tag{4.34}$$

(To motivate the rescaling of basal melt rate a_l, note that due to a phenomenon known as the *ice pump* (Holland & Jenkins 2001), a convection cell is often formed in the ocean waters below the shelf. This can lead to significant rates of melting far larger than surface snowfall [a]. Our rescaling of a_l above is chosen so that basal melting M can have a leading-order effect on the dynamics of the ice shelf; this contrasts with the normal stress boundary layer, in which accumulation rate is small in (4.23c). Below, we assume that $M(X,t)$ is a prescribed function.)

With these rescalings, the model (4.7)–(4.9) now becomes the following: (4.7)–(4.8) again take the form (4.22)–(4.23), while (4.9) becomes

$$(P + r^{-1}L - T_1)L_X + T_2 = 0, \tag{4.35a}$$

$$-P - r^{-1}L - T_1 - \nu'^2 T_2 L_X = 0, \tag{4.35b}$$

$$\varepsilon^{4/5} L_t - \varepsilon^{1/5}\dot{x}_g L_X + U L_X = V - M, \tag{4.35c}$$

$$L > B \tag{4.35d}$$

on $Z = L$, $X > 0$.

We can depth-integrate the shelf model ((4.22), (4.23) and (4.35)) using exactly the same steps that led to (4.29). From (4.25b) and $(4.26)_2$, we again have $P + T_1 = S - Z$. At leading order, we then have from (4.35b) that

$$H = S - L = -r^{-1}L, \quad S = (1-r)H. \tag{4.36a}$$

As before, $U = U(X,t)$ and $T_1 = 2U_X$ are independent of Z at leading order from (4.25e) and (4.25d). Substituting $P_X = S_X - T_{1,X}$ in (4.25a) and integrating the resulting equation as well as (4.25c) from $Z = L$ to $Z = S$ yields, on application of the appropriate boundary conditions as in the derivation of (4.29a) and (4.29b),

$$4(HU_X)_X - (1-r)HH_X = 0, \tag{4.36b}$$

$$(UH)_X = -M, \tag{4.36c}$$

$$H < -r^{-1}b(x_g) \tag{4.36d}$$

on $X > 0$. The model (4.36) can be recognized as the standard steady-state ice shelf model (e.g. MacAyeal & Barcilon 1988). As in the case of the normal stress boundary layer, the model above is a steady-state model because the advection time scale for the shelf ($= \varepsilon^{4/5}[t]$) is much shorter than for the outer region ($= [t]$).

Integrating (4.36b), we can find strain rate in terms of shelf thickness,

$$U_X = (1-r)H/8 + C/H, \tag{4.37}$$

where C is a constant of integration. Assuming that stress remains bounded as H becomes small, we obtain $C = 0$. Hence

$$U_X = (1-r)H/8, \tag{4.38}$$

and extensional stress

$$T_1 = 2U_X = (1-r)H/4 \tag{4.39}$$

is therefore determined by ice thickness alone. We note that this result is independent of the assumption that the ice shelf is in steady state.

We can go further and find a complete closed-form solution to (4.36) (see also van der Veen 1983). Integrating (4.36*c*), we find flux explicitly as

$$UH = Q_s(X,t), \quad Q_s(X,t) := Q_0 - \int_0^X M(X',t)\,\mathrm{d}X', \tag{4.40}$$

where $Q_0 = UH|_{X=0}$ is flux at the grounding line. Then we have $H = Q_s/U$, and the shelf must end at $X = X_c$ where $Q_s(x,t) = 0$. (In practice, it is more likely that the shelf will end at an $X < X_c$ where icebergs calve off, but this does not affect the calculation below.)

Putting $H = Q_s/U$ in (4.38),

$$U_X = \frac{(1-r)Q_s}{4U}, \tag{4.41}$$

so, by separation of variables,

$$U^2(X,t) = U_0^2(t) + \frac{(1-r)\int_0^X Q_s(X',t)\,\mathrm{d}X'}{2}, \tag{4.42}$$

where U_0 is ice velocity at the grounding line $X = 0$, and ice thickness can be found as $H = Q_s/U$.

Of course, Q_0 and U_0 in the shelf solution must be found through coupling with the normal stress boundary layer part of the grounded sheet. In fact, our main purpose here is not to calculate the shape of the ice shelf, but to use the ice shelf model to determine appropriate boundary conditions on (4.29) at the grounding line $X = 0$.

4.6. *Coupling the extensional stress boundary layer and shelf regions: continuity considerations and the role of the contact inequalities*

It is clear that the form of (4.36) is essentially the same as (4.29), apart from the absence of a friction term U in (4.36*b*) and the multiplication of the driving term $-HH_X$ in (4.36) by a buoyancy factor $(1-r)$. An obvious approach to coupling the two models is then to enforce continuity of ice velocity U (otherwise the gradient U_X would not be defined and extensional stress at the contact line would have to be infinite), ice flux UH (to ensure mass conservation) and the depth-integrated normal stress $\int_L^S T_1\,\mathrm{d}Z = 2HU_X$ (to ensure force balance). This is precisely what is done in Part 1, and it allows the boundary layer problem (4.29) to be closed.

Upstream of the grounding line, $X < 0$, we have $H \geqslant -r^{-1}b(x_g)$ from (4.29*c*) while on the downstream side, $X > 0$, we have $H < -r^{-1}b(x_g)$ from (4.35*d*). If U and UH are continuous at $X = 0$, then so is H, and this implies that ice thickness must be *at* the critical value for flotation at leading order,

$$H = -r^{-1}b(x_g) \quad \text{at } X = 0, \tag{4.43}$$

where we must of course have $b(x_g) < 0$, so the ice sheet bed at the grounding line is indeed below sea level. (Note that (4.29*c*) and (4.35*d*) are simply the leading-order

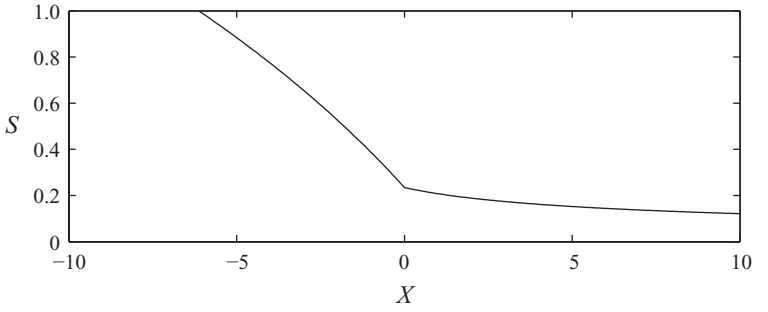

FIGURE 3. The solution S for surface elevation from §§ 4.3 and 4.5 plotted against X; here, we have $b(x_g) = 2.117$ corresponding to $Q = 1$ (see the Appendix for a method of computing Q as a function of $b(x_g)$) as well as $M = 0$. The most important feature of this graph is the break in slope at the contact line $X = 0$. The slope discontinuity only appears at this scale. When one zooms into the region around the slope break, a boundary layer ensures a continuous transition whose shape is given by figure 4(c).

versions of the contact inequalities (2.4d) and (2.5c), and we can see here how they determine ice thickness at the contact line.) Meanwhile, continuity of normal stress and (4.38) implies that

$$U_X = -\frac{(1-r)b(x_g)}{8r}, \quad \text{at } X = 0. \tag{4.44}$$

The two conditions (4.43) and (4.44) along with (4.33a) provide the required boundary conditions for the boundary-layer problem (4.29). Moreover, they reproduce the corresponding boundary conditions (3.40) in Part 1.

The solution of the boundary-layer problem (4.29) with the boundary conditions (4.33a), (4.43) and (4.44) then determines the relationship between ice flux Q and depth b in the boundary layer. This problem is exactly the same as that considered in Part 1 (with the Part 1 parameters $m = n = 1$). By continuity of flux, we must have $Q_0 = Q$, while continuity of velocity also gives us the constant of integration $U_0 = Q/[-r^{-1}B(x_g)]$ in the shelf solution (4.42). We will revisit the solution of (4.29) with (4.33a), (4.43) and (4.44) in § 5. Before we do so, there is a further complication to attend to.

The boundary conditions (4.43) and (4.44) are based on the continuity of flux UH, velocity U and the velocity gradient U_X across the grounding line. These continuity assumptions also imply that the thickness gradient $H_X = -HU_X/U$ is also continuous. Upstream of the grounding line, we however have that $S = H - b(x_g)$ and hence we have $S_X = H_X$. Downstream of the grounding line, we have flotation and hence $S = (1-r)H$, so $S_X = (1-r)H_X$. To show that this discontinuity in slope (see figure 3) does not invalidate the continuity assumptions leading to (4.43) and (4.44), we have to consider the transition from grounded to floating ice near the grounding line in greater detail.

4.7. *The slope boundary layer: a beam problem*

We seek an additional boundary layer just downstream of the grounding line that describes the continuous transition in vertical velocity and surface slope and from grounded sheet to floating shelf. As indicated in § 3, this slope boundary layer takes the form of a viscous beam problem.

The discontinuity in ice surface slope predicted above results from the requirement in (4.36a) that the ice shelf be afloat in the Archimedean sense. A continuous change

in surface slope across the grounding line therefore does not allow the flotation conditions (4.36*a*) to be satisfied exactly close to the grounding line. The associated departures from flotation then induce buoyancy effects that cause 'bending' of the shelf as a viscous beam and ultimately lead to a smooth transition in surface slope. Mechanically, this bending corresponds to horizontal gradients of shear stress $\partial\tau_2/\partial x$ playing a significant role.

In § 3, we motivated a length scale $\sim L_q^{27/25}L_s^{-2/25} = \varepsilon^{7/25}\nu'^{4/5}L = \varepsilon^{3/5}\nu'^{4/5}L$. As the length scale for the extensional stress boundary layer is $\varepsilon^{3/5}L$, this suggests that we rescale horizontal distance in the slope boundary layer as

$$X = \nu'^{4/5}\tilde{X}. \tag{4.45}$$

In addition, the rescalings required to describe the beam-like structure of the vertical velocity field V in the slope boundary layer are

$$U = \tilde{U}, \quad V = \tilde{V}, \quad P = \tilde{P}, \quad T_1 = \tilde{T}_1, \quad T_2 = \nu'^{-2/5}\tilde{T}_2, \tag{4.46}$$

$$L = \tilde{L}, \quad S = \tilde{S}. \tag{4.47}$$

We substitute these into (4.22), (4.23) and (4.35) for the floating portion of the ice,

$$\tilde{T}_{1,\tilde{X}} + \nu'^{2/5}\tilde{T}_{2,Z} - \tilde{P}_{\tilde{X}} = 0, \tag{4.48a}$$

$$-\tilde{T}_{1,Z} + \nu'^{4/5}\tilde{T}_{2,\tilde{X}} - \tilde{P}_Z - 1 = 0, \tag{4.48b}$$

$$\tilde{U}_{\tilde{X}} + \nu'^{4/5}\tilde{V}_Z = 0, \tag{4.48c}$$

$$2\tilde{U}_{\tilde{X}} = \nu'^{4/5}\tilde{T}_1, \tag{4.48d}$$

$$\tilde{U}_Z + \nu'^{6/5}\tilde{V}_{\tilde{X}} = \nu'^{8/5}\tilde{T}_2 \tag{4.48e}$$

on $\tilde{L} < Z < \tilde{S}$, and

$$\left(\tilde{P} - \tilde{T}_1\right)\tilde{S}_{\tilde{X}} + \nu'^{2/5}\tilde{T}_2 = 0, \tag{4.49a}$$

$$-\tilde{P} - \tilde{T}_1 - \nu'^{4/5}\tilde{T}_2\tilde{S}_{\tilde{X}} = 0, \tag{4.49b}$$

$$\nu'^{4/5}\varepsilon^{4/5}(\tilde{S}_t - a) + \varepsilon^{1/5}\dot{x}_g\tilde{S}_{\tilde{X}} + \tilde{U}\tilde{S}_{\tilde{X}} = \nu'^{4/5}V \tag{4.49c}$$

on $Z = \tilde{S}$, as well as

$$\left(\tilde{P} + r^{-1}\tilde{L} - \tilde{T}_1\right)\tilde{S}_{\tilde{X}} + \nu'^{2/5}\tilde{T}_2 = 0, \tag{4.50a}$$

$$-\tilde{P} - r^{-1}\tilde{L} - \tilde{T}_1 - \nu'^{4/5}\tilde{T}_2\tilde{S}_{\tilde{X}} = 0, \tag{4.50b}$$

$$\nu'^{4/5}\varepsilon^{4/5}\tilde{L}_t + \varepsilon^{1/5}\dot{x}_g\tilde{L}_{\tilde{X}} + \tilde{U}\tilde{L}_{\tilde{X}} = \nu'^{4/5}(V + M), \tag{4.50c}$$

$$\tilde{L} > b(x_g + \varepsilon^{3/5}\nu'^{4/5}\tilde{X}) \tag{4.50d}$$

on $Z = \tilde{L}$, $\tilde{X} > 0$.

Our aim here is to show that the boundary conditions (4.43) and (4.44) can be justified, and that a beam-like deformation of the shelf near the contact line alleviates the apparent problem of a discontinuous vertical velocity. To do so, we expand the dependent variables in powers of $\nu'^{2/5}$ as

$$\tilde{U} \sim \tilde{U}^{(0)} + \nu'^{4/5}\tilde{U}^{(2)} + \nu'^{6/5}\tilde{U}^{(3)} + O(\nu'^{8/5}), \quad \tilde{V} \sim \tilde{V}^{(0)} + O(\nu'^{2/5}), \tag{4.51}$$

$$\tilde{L} \sim \tilde{L}^{(0)} + \nu'^{4/5}\tilde{L}^{(2)} + O(\nu'^{6/5}), \quad \tilde{S} \sim \tilde{S}^{(0)} + \nu'^{4/5}\tilde{S}^{(2)} + O(\nu'^{6/5}), \tag{4.52}$$

$$\tilde{T}_1 \sim \tilde{T}_1^{(0)} + \nu'^{2/5}\tilde{T}_1^{(1)} + \nu'^{4/5}\tilde{T}_1^{(2)} + O(\nu'^{6/5}), \quad \tilde{T}_2 \sim \tilde{T}_2^{(0)} + O(\nu'^{2/5}), \tag{4.53}$$

$$\tilde{P} \sim \tilde{P}^{(0)} + \nu'^{2/5}\tilde{P}^{(1)} + \nu'^{4/5}\tilde{P}^{(2)} + O(\nu'^{6/5}), \tag{4.54}$$

where we have left out first-order terms in $\nu'^{2/5}$ in the expansions of U, S and L because these turn out to be zero and we do not wish to labour this point. We will see below that the expansions given above lead to well-posed higher-order equations and that there are therefore no missing terms in these expansions.

The leading-order forms of (4.48)–(4.50) are simple and we do not give them here to save space. Instead, we state the relevant results. From (4.48*d*), (4.48*e*), (4.49*c*) and (4.50*c*), $\tilde{U}^{(0)}$, $\tilde{L}^{(0)}$ and $\tilde{S}^{(0)}$ are all constants (independent of $\tilde{X}$ and Z) with $\tilde{S}^{(0)}$ and $\tilde{L}^{(0)}$ related through Archimedean flotation,

$$\tilde{S}^{(0)} = (1 - r^{-1})\tilde{L}^{(0)}. \tag{4.55}$$

Leading-order pressure is related to extensional stress from (4.48*b*) as

$$\tilde{P}^{(0)} = \tilde{S}^{(0)} - Z - \tilde{T}_1^{(0)}, \tag{4.56}$$

and from (4.48*a*) $\tilde{T}_1^{(0)}$ is independent of $\tilde{X}$. By matching with the shelf (which corresponds to the simultaneous limits $\tilde{X} \to \infty$, $X \to 0$), it is easy to show that

$$\tilde{U}^{(0)} = \lim_{X\to 0^+} U(X,t), \quad \tilde{T}_1^{(0)} = \lim_{X\to 0^+} T_1 = \lim_{X\to 0^+} 2U_X, \tag{4.57}$$

$$\tilde{S}^{(0)} = \lim_{X\to 0^+} S(X,t), \quad \tilde{L}^{(0)} = \lim_{X\to 0^+} L(X,t), \tag{4.58}$$

where 0^+ denotes the limit $X = 0$ approached from above (i.e. from within the shelf rather than the extensional stress boundary layer). At leading order, horizontal velocity $\tilde{U}^{(0)}$ and extensional stress $\tilde{T}_1^{(0)}$ are both constant in the beam region and equal to their near-contact line values in the shelf, while the same is also true for surface and base elevations, which are related through Archimedean flotation.

It is however precisely the deviation from Archimedean flotation that explains the smooth transition in surface slope from grounded sheet to floating shelf, and this must therefore appear in the beam region at higher order (see also Baral, Hutter & Greve 2001). We therefore expand the governing equations.

Expanding (4.48*d*) and (4.48*e*) gives at $O(\nu'^{4/5})$,

$$\tilde{U}_Z^{(2)} = 0, \quad \tilde{U}_{\tilde{X}}^{(2)} = \tfrac{1}{2}\tilde{T}_1^{(0)}, \tag{4.59}$$

so that $\tilde{U}^{(2)}$ depends only on $\tilde{X}$ and its gradient $\tilde{U}_{\tilde{X}}^{(2)}$ is constant (because $\tilde{T}_1^{(0)}$ is constant). Expanding (4.48*c*) yields at $O(\nu'^{4/5})$,

$$\tilde{U}_{\tilde{X}}^{(2)} + \tilde{V}_Z^{(0)} = 0, \tag{4.60}$$

so that

$$\tilde{V}^{(0)} = V_L(\tilde{X},t) - \tilde{U}_{\tilde{X}}^{(2)}(Z - \tilde{L}^{(0)}), \tag{4.61}$$

where V_L is vertical velocity at the lower boundary of the ice, and we have made use of the fact that $\tilde{U}_{\tilde{X}}^{(2)}$ is constant. Below, V_L will play the role usually played by vertical displacement of the centreline of an elastic beam in standard elastic beam theory.

Next, expanding (4.48*d*) and (4.48*e*) to $O(\nu'^{6/5})$ yields, respectively,

$$\tilde{U}_{\tilde{X}}^{(3)} = \tfrac{1}{2}\tilde{T}_1^{(1)}, \quad \tilde{U}_Z^{(3)} + \tilde{V}_{\tilde{X}}^{(0)} = 0, \tag{4.62}$$

Hence

$$\tilde{U}^{(3)} = V_{L,\tilde{X}}(Z-\tilde{L}^{(0)}) + U_L(\tilde{X},t), \quad \tilde{T}_1^{(1)} = 2\left[U_{L,\tilde{X}} - V_{L,\tilde{X}\tilde{X}}(Z-\tilde{L}^{(0)})\right], \tag{4.63}$$

where U_L denotes variations in velocity U at the base of the ice and is independent of Z.

Next, we consider how deviations from flotation affect the velocity field V_L. First, note that expanding (4.48*a*), (4.48*b*), (4.49*b*), (4.49*a*) and (4.50*a*) to $O(\nu'^{2/5})$ gives

$$\tilde{T}_{1,\tilde{X}}^{(1)} + \tilde{T}_{2,Z}^{(0)} - \tilde{P}_{\tilde{X}}^{(1)} = 0, \quad \tilde{T}_{1,Z}^{(1)} - \tilde{P}_Z^{(1)} = 0, \tag{4.64}$$

with $\tilde{T}_1^{(1)} + \tilde{P}^{(1)} = 0$ on $Z = \tilde{S}^{(0)}$ and $\tilde{T}_2^{(0)} = 0$ on $Z = \tilde{L}^{(0)}$ as well as on $Z = \tilde{S}^{(0)}$. Hence

$$\tilde{T}_2^{(0)} = -2\int_{\tilde{L}^{(0)}}^{Z} \tilde{T}_{1,\tilde{X}}^{(1)}(X,Z',t)\,\mathrm{d}Z', \quad \left[\int_{\tilde{L}^{(0)}}^{\tilde{S}^{(0)}} \tilde{T}_1^{(1)}\,\mathrm{d}Z\right]_{\tilde{X}} = \int_{\tilde{L}^{(0)}}^{\tilde{S}^{(0)}} \tilde{T}_{1,\tilde{X}}^{(1)}\,\mathrm{d}Z = 0. \tag{4.65}$$

Noting that there is no $O(\nu'^{2/5})$ correction to normal stress T_1 in the shelf from (4.22), (4.23) and (4.35), it follows from matching with the shelf that

$$\int_{\tilde{L}^{(0)}}^{\tilde{S}^{(0)}} \tilde{T}_1^{(1)}\,\mathrm{d}Z = 0. \tag{4.66}$$

Substituting for $\tilde{T}_1^{(1)}$ from (4.63) in (4.66), we find a relationship between U_L and V_L:

$$U_{L,\tilde{X}} = \tfrac{1}{2} V_{L,\tilde{X}\tilde{X}}(\tilde{S}^{(0)} - \tilde{L}^{(0)}). \tag{4.67}$$

Moreover, expanding (4.48*b*), (4.49*b*) and (4.50*b*) to $O(\nu'^{6/5})$ yields

$$\tilde{T}_{1,Z}^{(2)} + \tilde{P}_Z^{(2)} - \tilde{T}_{2,\tilde{X}}^{(0)} = 0, \tag{4.68}$$

with $\tilde{T}_1^{(2)} + \tilde{P}^{(2)} = (1-r^{-1})\tilde{L}^{(2)}$ on $Z = \tilde{L}^{(0)}$ and $\tilde{T}_1^{(2)} + \tilde{P}^{(2)} = \tilde{S}^{(2)}$ on $Z = \tilde{S}^{(0)}$. Integrating (4.68) from $Z = \tilde{L}^{(0)}$ to $Z = \tilde{S}^{(0)}$ and applying these boundary conditions yields

$$\int_{\tilde{L}^{(0)}}^{\tilde{S}^{(0)}} \tilde{T}_{2,\tilde{X}}^{(0)}\,\mathrm{d}Z = \tilde{S}^{(2)} - (1-r^{-1})\tilde{L}^{(2)}. \tag{4.69}$$

However, we have a prescription in (4.65) for $\tilde{T}_2^{(0)}$, and with this, we get

$$-2\int_{\tilde{L}^{(0)}}^{\tilde{S}^{(0)}} \int_{\tilde{L}^{(0)}}^{Z} \tilde{T}_{1,\tilde{X}}^{(1)}(X,Z',t)\,\mathrm{d}Z'\,\mathrm{d}Z = \tilde{S}^{(2)} - (1-r^{-1})\tilde{L}^{(2)}. \tag{4.70}$$

This is our basic beam problem: the left-hand side is the gradient of the shear force $\int_{\tilde{L}^{(0)}}^{\tilde{S}^{(0)}} \tilde{T}_2^{(0)}\,\mathrm{d}Z$ in the ice (Evatt & Fowler 2007), while the right-hand side describes a restoring force due to deviations from Archimedean flotation. Substituting for $\tilde{T}_1^{(1)}$ from (4.63) and (4.67) yields the beam equation for vertical velocity V_L:

$$-\frac{(\tilde{S}^{(0)} - \tilde{L}^{(0)})^3}{3} V_{L,\tilde{X}\tilde{X}\tilde{X}\tilde{X}} = \tilde{S}^{(2)} - (1-r^{-1})\tilde{L}^{(2)}, \tag{4.71}$$

where we can identify the constant coefficient $(\tilde{S}^{(0)} - \tilde{L}^{(0)})^3/3$ as a viscous flexural rigidity for the shelf. Note that we have constructed (4.71) from the equations for floating ice, and (4.71) therefore holds downstream of the contact line, $\tilde{X} > 0$.

It remains to link $\tilde{S}^{(2)}$ and $\tilde{L}^{(2)}$ back to velocity V_L through (4.49*c*) and (4.50*c*). From (4.61), we have $\tilde{V}^{(0)}|_{Z=\tilde{S}^{(0)}} - \tilde{V}^{(0)}|_{Z=\tilde{L}^{(0)}} = -\tilde{U}^{(2)}_{\tilde{X}}(\tilde{S}^{(0)} - \tilde{L}^{(0)})$. However, expanding (4.49*c*) and (4.50*c*) to $O(\nu'^{4/5})$, we find

$$\tilde{U}^{(0)}\tilde{S}^{(2)}_{\tilde{X}} = \tilde{V}^{(0)} \quad \text{on } Z = \tilde{S}^{(0)}, \quad \tilde{U}^{(0)}\tilde{L}^{(2)}_{\tilde{X}} = \tilde{V}^{(0)} - M \quad \text{on } Z = \tilde{L}^{(0)}. \tag{4.72}$$

From this and (4.61), the mean thinning rate for the ice shelf in the slope transition region can be found at this order:

$$\tilde{S}^{(2)}_{\tilde{X}} - \tilde{L}^{(2)}_{\tilde{X}} = -\frac{\tilde{U}^{(2)}_{\tilde{X}}(\tilde{S}^{(0)} - \tilde{L}^{(0)}) + M}{\tilde{U}^{(0)}}. \tag{4.73}$$

Differentiating (4.71) with respect to $\tilde{X}$ and using (4.73), we finally obtain a closed equation for V_L,

$$\frac{(\tilde{S}^{(0)} - \tilde{L}^{(0)})^3}{3} V_{L,\tilde{X}\tilde{X}\tilde{X}\tilde{X}\tilde{X}} + \frac{1}{r\tilde{U}^{(0)}} V_L = \frac{\tilde{U}^{(2)}_{\tilde{X}}(\tilde{S}^{(0)} - \tilde{L}^{(0)}) + (1 - r^{-1})M}{\tilde{U}^{(0)}}. \tag{4.74}$$

The base and surface slopes $\tilde{S}^{(2)}_{\tilde{X}}$ and $\tilde{L}^{(2)}_{\tilde{X}}$ can be reconstructed from the solution V_L to (4.74) through (4.61) and (4.72).

Note that the coefficients $\tilde{T}^{(0)}_1$, $\tilde{U}^{(0)}$, $\tilde{U}^{(2)}_{\tilde{X}}$, $\tilde{S}^{(0)}$ and $\tilde{L}^{(0)}$ in (4.74) are constants determined by coupling with the shelf problem through (4.58). Assuming that M is a function of the 'outer' ice shelf variable $X = \nu'^{4/5}\tilde{X}$, we also treat $M = M(\nu'^{4/5}\tilde{X}) \sim M(0)$ as a constant here. A solution is now straightforward to find, although by contrast with elastic beam equations, we have a fifth- rather than fourth-order differential equation. The general solution to (4.74) takes the form

$$V_L = r\left[\tilde{U}^{(2)}_{\tilde{X}}(\tilde{S}^{(0)} - \tilde{L}^{(0)}) + (1 - r^{-1})M\right] + \sum_{k=0}^{4} A_k\, \mathrm{e}^{m_k \tilde{X}}, \tag{4.75}$$

where we have defined

$$m_k = \left[\frac{3}{r\tilde{U}^{(0)}(\tilde{S}^{(0)} - \tilde{L}^{(0)})^3}\right]^{1/5} \mathrm{e}^{\mathrm{i}(2k+1)\pi/5}. \tag{4.76}$$

To solve the beam problem fully, we need to find the amplitudes A_k. This requires boundary conditions for (4.74). One set of boundary conditions is easy to find: as $\tilde{X} \to \infty$, we clearly need $V_L = \tilde{V}^{(0)}|_{Z=\tilde{L}^{(0)}}$ to remain bounded, so $A_0 = A_4 = 0$. In fact, by matching with the ice shelf, we expect from (4.35*c*) that

$$\lim_{\tilde{X}\to\infty} V_L(\tilde{X}, t) = \lim_{X\to 0}\left[V(X, Z, t)|_{Z=L(X,t)}\right] = \lim_{X\to 0}(UL_X - M). \tag{4.77}$$

However, in the shelf $L = -rH$ and from (4.36*c*), $UL_X = -rUH_X = r(U_X H + M)$, and so we expect

$$\lim_{\tilde{X}\to\infty} V_L = \lim_{X\to 0}[rU_X H - (1 - r)M]. \tag{4.78}$$

Bearing in mind (4.58), this is precisely what we obtain from (4.76) if the exponential terms in (4.76) tend to zero as $\tilde{X} \to \infty$, i.e. if only terms with $\mathrm{Re}(m_k) < 0$ are included in the sum over k. Hence $A_0 = A_4 = 0$.

This still leaves the coefficients A_1, A_2 and A_3 to be determined. We have already matched the beam problem successfully with the shelf solution, and the remaining coefficients can therefore be determined only by coupling the beam problem with the

extensional stress boundary layer that lies upstream of the contact line. We expect that this coupling takes the form of boundary conditions at $\tilde{X}=0$. However, asymptotic matching will not help us here: there is no overlap region between the beam and the extensional stress boundary layer, as they are subject to different boundary conditions at the base of the ice.

To match, we actually have to introduce yet another boundary layer that straddles the contact line itself. This boundary layer then not only determines the remaining coefficients A_1, A_2 and A_3, but also justifies the boundary conditions (4.43) and (4.44) on the extensional stress boundary layer: we have already seen that ice thickness, velocity and stress are constant at leading order in the beam region. The arguments leading up to (4.43) and (4.44) are then correct if the leading-order ice thickness, velocity and stress in the beam region are also continuous across the contact line. To show this requires the additional boundary layer straddling the contact line.

We will describe this boundary layer in the next section. For ease of presentation, we pre-empt its results here, and state the relevant boundary conditions on V_L that allow us to calculate A_1, A_2 and A_3 in (4.76). These are the boundary conditions one would also find at the contact line of an elastic beam (where V_L would have to be identified as displacement), namely

$$\lim_{\tilde{X}\to 0^+} V_L = \lim_{\tilde{X}\to 0^+} V_{L,\tilde{X}} = \lim_{\tilde{X}\to 0^+} V_{L,\tilde{X}\tilde{X}} = 0. \tag{4.79}$$

Of these, the first condition $\lim_{\tilde{X}\to 0} V_L = 0$ can be motivated easily. It shows that the beam region alleviates the problem of a discontinuous vertical velocity across the contact line $X=\tilde{X}=0$. From (4.49*c*) and (4.61), we have $\lim_{\tilde{X}\to 0^+} \tilde{S}^{(2)}_{\tilde{X}} = -\tilde{U}^{(2)}_{\tilde{X}}(\tilde{S}^{(0)} - \tilde{L}^{(0)})/\tilde{U}^{(0)} = -\lim_{X\to 0^+} U_X H/U = -\lim_{X\to 0^-} U_X H/U$ if velocity U, thickness H and velocity gradient U_X are continuous between the normal stress boundary layer and the ice shelf across $X=0$. In the normal stress boundary layer, $S_X = H_X = -U_X H/U$ from (4.29*b*), and hence $\lim_{\tilde{X}\to 0^+} \tilde{S}^{(2)}_{\tilde{X}} = \lim_{X\to 0^-} S_X$ as expected.

With the boundary conditions (4.79), the solution to (4.74) finally becomes

$$V_L = \left[r\tilde{U}^{(2)}_{\tilde{X}}(\tilde{S}^{(0)} - \tilde{L}^{(0)}) - (1-r)M\right] \times \left\{1 + \frac{\cos\left(\frac{3\pi}{5} + \bar{m}\sin\left(\frac{2\pi}{5}\right)\tilde{X}\right)\mathrm{e}^{-\bar{m}\cos(2\pi/5)\tilde{X}} - \cos\left(\frac{\pi}{5}\right)\mathrm{e}^{-\bar{m}\tilde{X}}}{2\sin\left(\frac{2\pi}{5}\right)\sin\left(\frac{\pi}{5}\right)}\right\}, \tag{4.80}$$

where

$$\bar{m} = \left[\frac{3}{r\tilde{U}^{(0)}(\tilde{S}^{(0)} - \tilde{L}^{(0)})^3}\right]^{1/5}. \tag{4.81}$$

The amplitude of variations in V_L is therefore set by melt rate M, ice thickness $\tilde{S}^{(0)} - \tilde{L}^{(0)}$ and horizontal velocity gradient $\tilde{U}^{(2)}_{\tilde{X}}$ near the grounding line. Spatially, variations in V_L take the form of an attenuated sine wave of fixed shape with a wavelength given by the parameter $\bar{m}$, which in turn depends only on the flexural rigidity $(\tilde{S}^{(0)} - \tilde{L}^{(0)})^3/3$ of the shelf and on the flow speed $\tilde{U}^{(0)}$. The form of V_L is illustrated in figure 4. From this solution, we can reconstruct the base elevation of the ice $\tilde{L}^{(2)}$ by integrating (4.50*c*) from $\tilde{X}=0$, where we expect the ice to make with

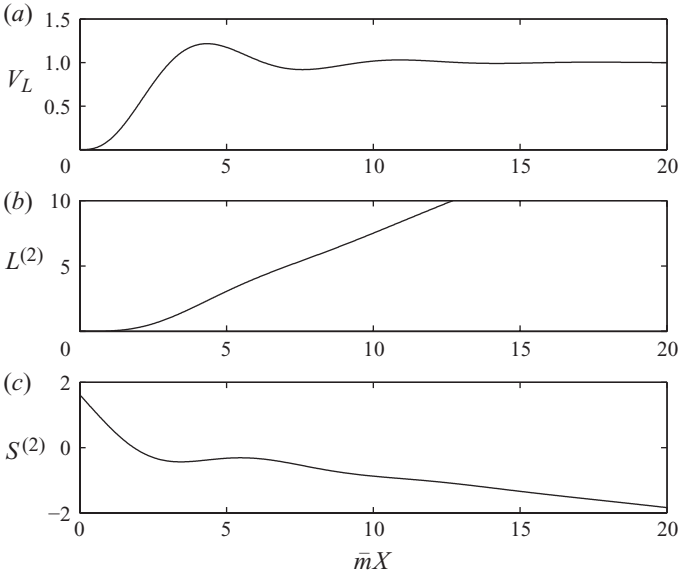

FIGURE 4. The attenuated sine wave form of $V_L(\tilde{X})$ given by (4.80) is plotted in (a) against the variable $\bar{m}\tilde{X}$ for the case of unit 'amplitude' $r\tilde{U}^{(2)}_{\tilde{X}}(\tilde{S}^{(0)}-\tilde{L}^{(0)})-(1-r)M=1$. Note that the shape of the wave is independent of any of the model parameters (in particular, it does not depend on $\bar{m}$, which only determines its wavelength). The corresponding base and surface elevation are plotted in (b) and (c) for the case $M=0$, in both cases normalized by $\tilde{U}^{(0)}_{\tilde{X}}(\tilde{S}^{(0)}-\tilde{L}^{(0)})/(\bar{m}\tilde{U}^{(0)})$. Note that the second-order surface correction $\tilde{S}^{(2)}$ shown in (c) has a noticeable surface bump with an adverse slope around $\bar{m}X=4$. A similar surface feature has been found by Durand *et al.* (2009), see the inset of their figure 2. It is clear that $\tilde{S}^{(2)}$ shown in (c) represents a transition from a steep slope at $X=0$ to a less steep one as $X\to\infty$; this is what happens close to the break in slope in figure 3.

contact with the bed, so $\tilde{L}^{(2)}|_{\tilde{X}=0}=0$:

$$\tilde{L}^{(2)}(\tilde{X},t)=\frac{1}{\tilde{U}^{(0)}}\int_0^{\tilde{X}} V_L(\tilde{X}',t)+M\,\mathrm{d}\tilde{X}'. \tag{4.82}$$

We have so far not considered the contact inequality (4.50d) here. Anticipating that the arguments in §4.6 hold, we will have $\tilde{L}^{(0)}=\lim_{X\to 0^+}L=b(x_g)$, in which case (4.50$d$) requires $\tilde{L}^{(2)}>0$. This is satisfied by the solution above: with $M>0$ and $V_L>0$ (see figure 4) it follows from (4.82) that $\tilde{L}^{(2)}>0$, and hence the inequality (4.50d) will be satisfied. Given a solution for $\tilde{L}^{(2)}$, the surface elevation $\tilde{S}^{(2)}$ can then be recovered from (4.71). In particular, the non-zero deviation of ice thickness from Archimedean flotation at the grounding line can now be computed at $O(\nu'^{4/5})$ as

$$\tilde{S}^{(2)}|_{\tilde{X}=0}=-\frac{2(\tilde{S}^{(0)}-\tilde{L}^{(0)})^3}{3}\,V_{L,\tilde{X}\tilde{X}\tilde{X}\tilde{X}}\big|_{\tilde{X}=0}=\frac{\big(r\tilde{U}^{(2)}_{\tilde{X}}\big(\tilde{S}^{(0)}-\tilde{L}^{(0)}\big)-(1-r)M\big)}{2(1+\sqrt{5})r\tilde{U}^{(0)}\bar{m}}. \tag{4.83}$$

This confirms the observation of Durand *et al.* (2009) that ice thickness at the grounding line is not exactly equal to the critical value for flotation.

4.8. *The contact line boundary layer*

As we have just seen, the slope boundary layer cannot be matched directly to the extensional stress boundary layer. Coupling between these two regions requires yet another boundary layer straddling the contact line itself. This boundary layer then captures the switch in boundary conditions and can match to the slope and extensional stress boundary layers. The horizontal extent of this contact line boundary layer is ice thickness itself. Close to the grounding line, we therefore rescale horizontal distance in order to describe a region whose horizontal extent is comparable with its vertical extent. As ν' is the aspect ratio of the extensional stress boundary layer, in which X denotes horizontal distance from the grounding line, this rescaling takes the form

$$\hat{X} = X/\nu' = \tilde{X}/\nu'^{1/5}. \tag{4.84}$$

(Recall that a tilde refers to variables scaled for the slope boundary layer, while undecorated upper case variables refer to either the shelf or the extensional stress boundary layer. We will use hat decorations to denote variables in the contact line boundary layer.) To accommodate stresses due to the slope boundary layer, we further define

$$U = \hat{U}, \quad V = \hat{V}, \quad T_1 = \hat{T}_1, \quad T_2 = \nu'^{-1}\hat{T}_2, \quad P = \hat{P}, \quad S = \hat{S}, \quad L = \hat{L}, \tag{4.85}$$

so that $\hat{T}_2 = \nu'^{-3/5}\tilde{T}_2$; this indicates that the boundary layer is essentially a shear stress boundary layer. The model (4.7)–(4.10) then becomes

$$\hat{T}_{1,\hat{X}} + \hat{T}_{2,Z} - \hat{P}_{\hat{X}} = 0, \tag{4.86a}$$

$$-\hat{T}_{1,Z} + \hat{T}_{2,\hat{X}} - \hat{P}_Z = 0, \tag{4.86b}$$

$$\hat{U}_{\hat{X}} + \nu'\hat{V}_Z = 0, \tag{4.86c}$$

$$2\hat{U}_{\hat{X}} = \nu'\hat{T}_1, \tag{4.86d}$$

$$\hat{U}_Z + \nu'\hat{V}_{\hat{X}} = \nu'\hat{T}_2, \tag{4.86e}$$

$$\tag{4.86f}$$

on $\hat{L} < Z < \hat{S}$, with

$$(\hat{P} - \hat{T}_1)\hat{S}_{\hat{X}} + \hat{T}_2 = 0, \tag{4.87a}$$

$$-\hat{P} - \hat{T}_1 - \hat{T}_2\hat{S}_X = 0, \tag{4.87b}$$

$$\nu'\varepsilon^{4/5}(\hat{S}_t - a) - \varepsilon^{1/5}\dot{x}_g\hat{S}_{\hat{X}} + \hat{U}\hat{S}_{\hat{X}} = \nu'\hat{V}, \tag{4.87c}$$

on $Z = \hat{S}$, and

$$(\hat{P} + r^{-1}\hat{L} - \hat{T}_1)\hat{L}_{\hat{X}} + \hat{T}_2 = 0, \tag{4.88a}$$

$$-\hat{P} - r^{-1}\hat{L} - \hat{T}_1 - \hat{T}_2\hat{L}_{\hat{X}} = 0, \tag{4.88b}$$

$$\nu'\varepsilon^{4/5}\hat{L}_t - \varepsilon^{1/5}\dot{x}_g\hat{L}_{\hat{X}} + \hat{U}\hat{L}_{\hat{X}} = \nu'(\hat{V} + M), \tag{4.88c}$$

$$\hat{L} > B \tag{4.88d}$$

on $Z = \hat{L}$, $\hat{X} > 0$, as well as

$$\frac{-2\nu'\varepsilon^{3/5}b_x\hat{T}_1 + \left(1 - \nu'^2\varepsilon^{6/5}b_x^2\right)\hat{T}_2}{1 + \nu'^2\varepsilon^{6/5}b_x^2} = \nu'\left(1 + \nu'^2\varepsilon^{6/5}b_x^2\right)^{1/2}\hat{U}, \tag{4.89a}$$

$$\hat{V} = \varepsilon^{3/5}\hat{U}b_x, \tag{4.89b}$$

$$\hat{P} + \frac{\left(1 - \nu'^2\varepsilon^{6/5}b_x^2\right)\hat{T}_1 + 2\nu'\varepsilon^{3/5}b_x\hat{T}_2}{1 + \nu'^2\varepsilon^{6/5}b_x^2} \geqslant -r^{-1}b, \tag{4.89c}$$

on $Z = b$, $\hat{X} < 0$, while $\hat{L} = b$ for $\hat{X} \leqslant 0$ and $\hat{L}$ is continuous at $\hat{X} = 0$.

As in the slope boundary layer, it is again straightforward to show that the leading-order horizontal velocity, surface and base elevations are constant. For velocity $\hat{U}$, this follows from (4.86*d*) and (4.86*e*), while for surface and base elevations, it follows from (4.87*c*), (4.88*c*) and the continuity of $\hat{L}$ at the grounding line $\hat{X} = 0$. Together with the fact that $\tilde{U}^{(0)}$, $\tilde{S}^{(0)}$ and $\tilde{L}^{(0)}$ are constant in the slope boundary layer, these results justify the continuity of velocity and ice thickness between the extensional stress boundary layer and the shelf postulated in § 4.6. Formally, putting $\hat{U} = \bar{U} + O(\nu')$, $\hat{S} = \bar{S} + O(\nu')$, $\hat{L} = \bar{L} + O(\nu')$, we get velocity continuity by matching with the extensional stress and slope boundary layers: $\bar{U} = \lim_{\tilde{X}\to 0^+} \tilde{U}^{(0)} = \lim_{X\to 0^+} U = \lim_{X\to 0^-} U$. (Recall again that tildes refer to the slope boundary layer and undecorated variables refer to extensional stress boundary layer and ice shelf.) Similarly, by matching $\bar{S}$ and $\bar{L}$ with the extensional stress and beam boundary layers, we obtain thickness continuity: $\bar{L} = b(x_g) = \tilde{L}^{(0)} + \nu'^{4/5}\tilde{L}^{(2)}|_{\tilde{X}=0} = \tilde{L}^{(0)}$ (because $\tilde{L}^{(2)}|_{\tilde{X}=0} = 0$ in § 4.7) and $\lim_{X\to 0^-} S = \bar{S} = \tilde{S}^{(0)} + \nu'^{4/5}\tilde{S}^{(2)}|_{\tilde{X}=0}$. However, $\tilde{S}^{(0)} = \lim_{X\to 0^+} S(X, t)$ and $\tilde{L}^{(0)} = \lim_{X\to 0^+} L(X, t)$. Therefore, surface and base elevation, and hence ice thickness, is also continuous to leading order as in (4.43).

We still need to justify continuity of extensional stress between the ice shelf and the extensional stress boundary layer to justify (4.44). This is a simple question of force balance. With $\hat{S} = \bar{S}$ and $\hat{L} = \bar{L}$ constant to $O(\nu')$ and hence $\hat{S}_{\hat{X}} = \hat{L}_{\hat{X}} = 0$ to $O(\nu')$, the boundary conditions (4.87*a*), (4.88*a*) and (4.89*a*) become $\hat{T}_2 = 0$ to $O(\nu')$ on $Z = \bar{S}$ and $Z = \bar{L}$. Integrating (4.86*a*) over a rectangle $-R < X < R$, $\bar{L} < Z < \bar{S}$ and applying the divergence theorem then yields, to an error $O(\nu')$,

$$\int_{\bar{L}}^{\bar{S}} (\hat{T}_1 - \hat{P})|_{\hat{X}=-R}\,\mathrm{d}Z = \int_{\bar{L}}^{\bar{S}} (\hat{T}_1 - \hat{P})|_{\hat{X}=-R}. \tag{4.90}$$

However, matching with the extensional stress boundary layer shows that $\hat{T}_1 - \hat{P} \sim \lim_{X\to 0^-} 2T_1$ as $\hat{X} \to -\infty$, while matching with the slope boundary layer demands $\hat{T}_1 - \hat{P} \sim \lim_{\tilde{X}\to 0^-} 2\tilde{T}_1$ as $\hat{X} \to \infty$. Hence, $\lim_{X\to 0^-} T_1 = \lim_{X\to 0^+} T_1$, and the boundary condition (4.44) follows.

The only thing that remains is to justify the boundary conditions (4.79) on the beam equation (4.74). This is a fairly technical problem that requires us to consider higher-order terms in (4.86)–(4.89). We only sketch the relevant treatment below and defer a full solution to a separate publication (C. Schoof, 2011, in preparation).

The higher-order terms that we consider are those needed to match with the vertical velocity field $\tilde{V}^{(0)} = V_L(\tilde{X}, t) - \tilde{U}_{\tilde{X}}^{(2)}(Z - \tilde{L}^{(0)})$ in the beam boundary layer. If we do not assume for the time being that the boundary conditions (4.79) on the beam problem necessarily hold, then, by matching with the slope boundary layer, the far-field vertical velocity in the contact line boundary layer studied in this section has to behave as

$$\hat{V}|_{Z=0} \sim \sum_{n=0}^{5} \nu'^{n/5} \left.\frac{\mathrm{d}^n V_L}{\mathrm{d}x^n}\right|_{\tilde{X}=0} \hat{X}^n + o(\nu') \tag{4.91}$$

as $\hat{X} \to \infty$. In other words, the vertical velocity field in the contact line boundary layer is linked to the vertical velocity field in the beam boundary layer near the contact

line $\tilde{X}=0$. In particular, to show that the boundary conditions (4.79) do hold, we have to show that the terms with $n=0,1,2$ in (4.91) must vanish, and while those with $n=3,4,5$ can, and in general will, be non-zero.

Equation (4.91) along with the results for $\hat{U}$, $\hat{S}$ and $\hat{L}$ then suggests that an appropriate expansion for the solution to (4.86)–(4.89) takes the form

$$U \sim \bar{U} + \nu' \sum_{n=0}^{5} \nu'^{n/5} \hat{U}^{(n)} + o(\nu'^2), \quad V \sim \sum_{n=0}^{5} \nu'^{n/5} \hat{V}^{(n)} + o(\nu'), \tag{4.92}$$

$$\left.\begin{aligned} T_1 &\sim \sum_{n=0}^{5} \nu'^{n/5} \hat{T}_1^{(n)} + o(\nu'), \quad T_2 \sim \hat{T}_2^{(0)} + \sum_{n=1}^{5} \nu'^{n/5} \hat{T}_+^{(n)} o(\nu'), \\ P &\sim (S-Z) + \hat{P}^{(0)} + \sum_{n=1}^{5} \nu'^{j/5} \hat{L}^{(n)} + o(\nu'), \end{aligned}\right\} \tag{4.93}$$

$$S \sim \tilde{S}^{(0)} + \nu'^{4/5} \tilde{S}^{(2)}|_{\tilde{X}=0} + \nu' \hat{S}^{(5)} + o(\nu'), \quad L \sim \bar{L} + \nu' \sum_{n=0}^{5} \nu'^{n/5} \hat{L}^{(n)}) + o(\nu'^2). \tag{4.94}$$

To write the expanded form of (4.86)–(4.89) in more succinct form, we put $\hat{\boldsymbol{U}}^{(n)} = (\hat{U}^{(n)}, \hat{V}^{(n)})$. Omitting the superscripts (n) for simplicity, the nth-order expansion of (4.86)–(4.89) can then be written in the standard Stokes problem form

$$\nabla^2 \hat{\boldsymbol{U}} - \nabla \hat{P} = \boldsymbol{0} \quad \text{on } B < Z < \hat{S}^{(0)}, \tag{4.95a}$$

$$\nabla \cdot \hat{\boldsymbol{U}} = 0 \quad \text{on } B < Z < \hat{S}^{(0)}, \tag{4.95b}$$

$$\hat{U}_Z + \hat{V}_{\hat{X}} = 0 \quad \text{on } Z = \hat{S}^{(0)}, \tag{4.95c}$$

$$\hat{P} - 2\hat{W}_Z = \begin{cases} 0, & n < 4, \\ \tilde{S}^{(2)}_{\tilde{X}=0}, & n = 4, \\ \displaystyle\int_0^{\hat{X}} \hat{V}^{(0)}|_{Z=\hat{S}^{(0)}} \, \mathrm{d}\hat{X}', & n = 5, \end{cases} \quad \text{on } Z = \hat{S}^{(0)}, \tag{4.95d}$$

$$\hat{U}_Z + \hat{V}_{\hat{X}} = 0 \quad \text{on } Z = B, \ \hat{X} > 0, \tag{4.95e}$$

$$\hat{P} - 2\hat{W}_Z = 0 \quad \text{on } Z = B, \ \hat{X} > 0, \tag{4.95f}$$

$$\hat{U}_Z + \hat{V}_{\hat{X}} = \begin{cases} 0 & n < 5, \\ \bar{U} & n = 5, \end{cases} \quad \text{on } Z = B, \ \hat{X} < 0, \tag{4.95g}$$

$$\hat{V} = 0 \quad \text{on } Z = B, \ \hat{X} < 0, \tag{4.95h}$$

together with the contact line inequalities

$$\left.\begin{aligned} \sum_{n=0}^{5} \nu'^{n/5} (\hat{P} - 2\hat{W}_Z)|_{Z=B} &\geqslant 0, \quad \text{for } \hat{X} < 0, \\ \int_0^{\hat{X}} M(\hat{X}') \, \mathrm{d}\hat{X}' + \sum_{n=0}^{5} \nu'^{n/5} \int_0^{\hat{X}} \hat{V}^{(n)}|_{Z=B} \, \mathrm{d}\hat{X}' &\geqslant 0, \quad \text{for } \hat{X} > 0. \end{aligned}\right\} \tag{4.95i}$$

Moreover, matching with slope boundary layer gives (4.91), or, reintroducing the superscripts (n),

$$\hat{V}^{(n)}|_{Z=0} \sim \left.\frac{\mathrm{d}^n V_L}{\mathrm{d}x^n}\right|_{\tilde{X}=0} \hat{X}^n, \tag{4.95j}$$

as $\hat{X} \to +\infty$, while matching with the extensional stress boundary layer yields $\hat{\boldsymbol{U}}^{(n)} \sim 0$ as $\hat{X} \to -\infty$ for $n < 5$, and $\hat{\boldsymbol{U}}^{(n)}$ given by a shearing profile (determined by the $O(\nu')$ correction to the leading-order extensional stress boundary layer problem in § 4.3) for $n = 5$.

This set of Stokes flow contact problems posed on a strip turns out to be tractable (though still non-trivially) by the Wiener–Hopf method. We will show in a separate paper (C. Schoof, 2011, in preparation) that the far-field conditions $\hat{V}|_{Z=B} \sim \hat{C}^{(n)} X^n$ indeed require the coefficient $\hat{C}^{(n)}$ to vanish for $n = 0, 1, 2$ (leading to trivial solutions for $\hat{\boldsymbol{U}}^{(n)}$) provided that M vanishes rapidly enough close to the contact line (which is physically reasonable as melting occurs due to the advection of warm water, which must be suppressed as the water-filled gap between ice and bed pinches out as the contact line is approached). Meanwhile, non-vanishing $\hat{C}^{(n)}$ are possible for $n = 3, 4, 5$. This then justifies the boundary conditions (4.79) for the beam problem and ensures that the solution to the slope boundary layer is unique, which was what we aimed to demonstrate in this section.

5. The outer problem revisited

Having gone through a detailed treatment of the boundary layer structure of a marine ice sheet, we summarize our results here and reconsider the outer problem. The outer problem (4.16) is a standard, diffusive thin-film free surface flow with shear and basal slip contributing to flux:

$$s_t - \left[s^2 s_x + \frac{\nu^2}{3\varepsilon} s^3 s_x\right]_x = a, \tag{5.1}$$

where s is surface elevation. Note that s can simultaneously be identified as ice thickness because the topography $b(x)$ of the ice sheet bed is assumed to be small compared with ice thickness. This problem is essentially of the same form as that studied in Part 1 and subsequently in Schoof (2007*a*) (both of which allowed for power-law constitutive relations). The only additional feature of (5.1) is that it allows shearing in the ice, unlike the model in Part 1.

Equation (5.1) is posed as a moving boundary problem on the domain $(0, x_g(t))$, where the contact line location x_g can evolve over time. To close the outer problem, two boundary conditions are required at $x = x_g(t)$, and these are supplied by matching with the extensional stress boundary-layer problem as outlined in §§ 4.3 and 4.4. The boundary conditions that apply to the outer problem are then

$$s(x_g, t) = 0, \quad q(x_g, t) = Q(b(x_g(t))), \tag{5.2}$$

where $q = -s^2 s_x - (\nu^2 \varepsilon^{-1}/3) s^3 s_x$ is ice flux and $Q(b(x_g))$ is a function that must be supplied from the solution of the extensional stress boundary-layer problem, which we can state in the form of (4.29) with boundary conditions (4.43), (4.44) and (4.33*a*).

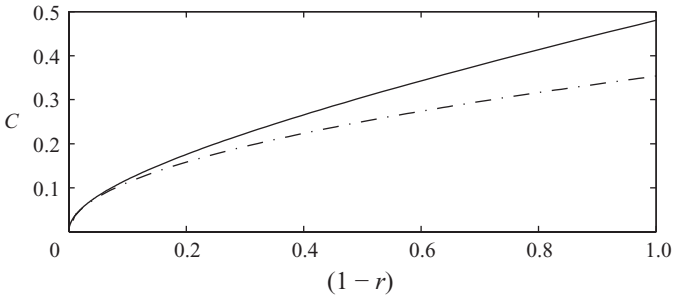

FIGURE 5. The coefficient C in (5.4) as a function of the flotation coefficient $(1-r)$ shown by a solid line, computed as described in the Appendix. The asymptotic result $C \sim ((1-r)/8)^{1/2}$ is shown by a dashed line; clearly, this agrees with the numerically computed values of C only for small $(1-r)$.

In other words, $Q(b(x_g))$ is determined by the nonlinear eigenvalue problem

$$4(HU_X)_X - U - HH_x = 0, \qquad -\infty < X < 0, \tag{5.3a}$$

$$UH = Q, \qquad -\infty < X < 0, \tag{5.3b}$$

$$U \to 0, \qquad \text{as } X \to -\infty, \tag{5.3c}$$

$$U \sim -HH_X, \qquad \text{as } X \to -\infty, \tag{5.3d}$$

$$H = -r^{-1}b(x_g), \qquad \text{at } X = 0, \tag{5.3e}$$

$$U_X = -(1-r)b(x_g)/(8r), \qquad \text{at } X = 0. \tag{5.3f}$$

The most important quality of the boundary conditions (5.2) is that the flux $q = Q(b(x_g))$ at the grounding line can be computed from the bed elevation $b(x_g)$ alone. In fact, it is possible to show that

$$Q = C\left(-\frac{b(x_g)}{r}\right)^{5/2}, \tag{5.4}$$

where C is a constant that depends only on m, n and r. This result corrects an assertion made in Part 1, namely that Q behaves as $\sim ((1-r)/8)^{1/2}(-b(x_g)/r)^{5/2}$ when $b(x_g)$ is small: the correct form of this statement would have been that (5.4) holds for *all* $b(x_g) < 0$ and that $C \sim ((1-r)/8)^{1/2}$ when $(1-r) \ll 1$ (see figure 5). In fact, Part 1 presented a partial treatment of a more general version of the boundary-layer problem (5.3), outlining how the flux Q at the grounding line can in principle be computed. A more complete analysis, including the derivation of (5.4), can be found in the Appendix.

6. Discussion and conclusions

In this paper, we have taken a first-principles approach to the fluid dynamics underlying marine ice sheet flow. We have used this to confirm the earlier results of Schoof (2007*b*) (Part 1) using matched asymptotic expansion techniques. In particular, we have shown that the boundary-layer structure for extensional stress near the grounding line predicted by Schoof (2007*b*) is preserved when considering a full Stokes flow model for the marine ice sheet rather than the simplified, depth-integrated model used in Schoof (2007*b*). This is consistent with the direct numerical results recently presented by Durand *et al.* (2009), who also confirm the earlier theory in Schoof (2007*b*).

The fact that the boundary-layer structure first presented in Schoof (2007*b*) is preserved implies that the qualitative behaviour for marine ice sheets outlined in that paper and also in Schoof (2007*a*) is confirmed by the results of the present study. The large-scale (outer) flow of the ice sheet can be described by a classical lubrication approximation (a 'shallow ice model' in glaciological parlance), and the interactions with the ice shelf at the grounding line can be represented through two boundary conditions that effectively parameterize extensional stress continuity and incipient flotation. One of these boundary conditions constrains ice thickness at the grounding line, while the other gives ice flux through the grounding line as a function of depth to bedrock there. The implications of these boundary conditions in terms of the local uniqueness, stability and bifurcations of steady states have been explored in Schoof (2007*a*), and the results presented there carry over to the model derived here, which differs only through including a representation of shearing in the outer flow.

In addition to the boundary-layer structure already described in Schoof (2007*b*), we have however also discovered two additional boundary layers very close to the grounding line that are passive in the large-scale dynamics of the ice sheet but account for the transition from grounded to floating ice in more detail. In particular, these extra boundary layers are necessary to explain the transition from a steep surface slope of the grounded ice near the grounding line to a much less steep surface slope on the ice shelf across a transition region in which there are noticeable surface undulations near the grounding line, some of them even with reversed surface slopes as shown in a recent numerical study by Durand *et al.* (2009). In this paper, we have shown that these undulations can be explained by the beam-like behaviour of the shelf very close to the grounding line.

The parameter regime in which the theory in Part 1 applies is also constrained more tightly by our work here. In addition to the small stress ratio ε that underpins the theory in Part 1, we find a second constraint on the aspect ratio ν of the ice sheet, which must be much smaller than $\varepsilon^{2/5}$. For the case of linear constitutive relations considered in this paper, this constraint can equally be re-written as a constraint on intrinsic length scales associated with shearing and sliding: we require the intrinsic scale for sliding L_s defined in § 3 to be much larger than the intrinsic scale for shearing L_q.

When this second constraint is not satisfied, the outer flow may still be a lubrication flow (which requires only $\nu \ll 1$ rather than the more restrictive $\nu \ll \varepsilon^{5/2} \ll 1$), but the extensional stress boundary layer near the contact line will no longer have a low aspect ratio ν'. In that case, the various boundary layers addressed in this paper (which are scale separated only when this aspect ratio is small) will coalesce. The transition from sheet to shelf is then likely to involve a single boundary layer whose aspect ratio is of order unity, as in Chugunov & Wilchinsky (1996) and Nowicki & Wingham (2008). When $\nu' \ll 1$, the shearing term in (4.16) will also dominate throughout the outer region, so the breakdown of the theory presented in this paper is linked intrinsically to the absence of a zone with strong sliding, and is physically likely to apply to ice masses frozen to their beds. A direct numerical approach (Durand *et al.* 2009) is typically required to solve the boundary-layer problem in this case, whereas the parameter regime considered here has the advantage of being tractable at least semi-analytically, with mechanical phenomena such as bending and the transition from an extensional- to a shear-stress-dominated flow occurring on distinct length scales.

In closing, we note that we have made some rather specific assumptions about bed topography in this paper. Specifically, it should scale as $[b] = \varepsilon^{1/5}[h] = L_q^{6/5} L_s^{-1/5}$, where $[h]$ is ice thickness in the outer region and ε a small stress ratio; $[b]$ is therefore

small compared with the ice thickness $[h] = (L_q^3 L/L_s)^{1/3}$ (see § 3). The boundary-layer problem (5.3) then produces an $O(1)$ flux $Q(b(x_g))$ through the grounding line for an $O(1)$ value of $b(x_g) < 0$, which is the dynamically most relevant scenario. There are other scenarios, which would translate into either large or small $b(x_g)$ in the boundary-layer problem (5.3). With $b(x_g)$ large, mass loss through the contact line as predicted by (5.4) necessarily exceeds the rate of accumulation over the ice sheet, and the ice sheet will necessarily shrink until the contact line reaches a position where b is not large. For sufficiently large $b(x_g)$, this shrinkage will occur extremely rapidly, with the interior of the ice sheet experiencing negligible elevation change while the contact line retreats. This scenario is explored in greater detail in §§ 3.1 and 3.2 of Part 1. An extreme case would be a steep drop-off from a bed that is above sea level inland from the grounding line to a bed that is deep offshore. In that case, the location of the grounding line is given at leading order by the location of the drop-off, and the flux through the grounding line is then primarily given by accumulation inland up to the location of the drop-off. Instead of determining the evolution of the ice mass, the boundary condition (5.2) then merely serves to determine the exact location of the grounding line close to the drop-off as a function of the prescribed flux.

By contrast, the case of small $b(x_g)$ corresponds to $Q \ll 1$. This essentially turns the marine ice sheet model into a model for a land-terminating ice sheet, in the sense that the boundary conditions for a land-terminating ice sheet at the ice margin are precisely of the form (5.2) with $Q = 0$. Neither of these cases is of much dynamic interest, which is why we chose the distinguished limit that leads to $Q = O(1)$.

This work was supported by a Canada Research Chair at the University of British Columbia, by NSERC Discovery Grant no. 357193-08 and by the Canadian Foundation for Climate and Atmospheric Science through the Polar Climate Stability Network. Many thanks to Gaël Durand for sharing his data and insights, to Eric de Giuli for pointing me to much of the literature on centre manifolds, and to Sophie Nowicki and Duncan Wingham for discussions. This manuscript was improved by the comments of the editor, Grae Worster, as well as those of the referees.

Appendix. The solution of the extensional stress boundary-layer problem

In this appendix, we present a mathematical analysis of the extensional stress boundary-layer problem (5.3) that controls the flux $Q(b(x_g))$ at the contact line. Instead of (5.3) we use the more general form of this problem first derived in Part 1 (where the signs of X and $B = b(x_g)$ were reversed from the present paper):

$$4\left(\frac{Q}{U}|U_X|^{1/n-1}U_X\right)_X - |U|^{m-1}U - \frac{Q}{U}\left(\frac{Q}{U}\right)_X = 0, \quad \text{for } X < 0 \tag{A 1a}$$

$$|U_X|^{1/n-1}U_X = -(1-r)B/(8r), \quad \text{at } X = 0 \tag{A 1b}$$

$$U = -rQ/B, \quad \text{at } X = 0 \tag{A 1c}$$

$$U \to 0, \quad \text{as } X \to -\infty \tag{A 1d}$$

$$|U|^{m-1}U \sim (Q/U)(Q/U)_X, \quad \text{as } X \to -\infty, \tag{A 1e}$$

where m, n are positive rheological constants, and the matching condition (A 1e) results from the lubrication flow behaviour $|U|^{m-1}U \sim -HH_X$ in the matching region with $H = Q/U$. Setting $m = n = 1$ gives the extensional stress boundary-layer problem (5.3) considered in this paper (with $H = Q/U$). In addition, we know that Q is positive

from matching with the outer problem, while $H \geqslant -B/r > 0$ in the boundary layer to satisfy the contact condition, so $U = Q/H > 0$.

We can show that B and Q enter into this problem only through

$$\theta = -r\,Q^{(m+1)/(n+m+3)}/B, \tag{A 2}$$

but not separately by rescaling

$$U = Q^{(n+2)/(n+m+3)}\mathscr{U}, \quad X = Q^{(2-nm)/(n+m+3)}\mathscr{X}, \tag{A 3}$$

which retrieves (A 1) with Q set to unity, B/r replaced by θ, U replaced by $\mathscr{U}$ and X by $\mathscr{X}$. Here show that this problem is solvable only for a unique value of θ (depending only on r), so that for a given density ratio r,

$$Q = \theta^{(m+n+3)/(m+1)}\,(-B/r)^{(m+n+3)/(m+1)}, \tag{A 4}$$

furnishes a unique relationship between flux Q and depth to bedrock B at the grounding line. Equation (5.4) is a special case of this, with $m = n = 1$. Moreover, we show that θ increases with $\delta = (1 - r)$, and that for small δ,

$$\theta \sim \left(\frac{\delta}{8}\right)^{n/(n+m+3)}. \tag{A 5}$$

To do so, we switch to slightly different phase plane variables from Part 1:

$$\xi = \mathscr{U}^{(m+n+3)/n}, \quad \Psi = \frac{|\mathscr{U}_{\mathscr{X}}|^{1/n-1}\mathscr{U}_{\mathscr{X}}}{\mathscr{U}^{(m+3)/n}}. \tag{A 6}$$

To be definite, since $\mathscr{U} > 0$, we restrict ξ to be non-negative, and Ψ to have the same sign as $\mathscr{U}_{\mathscr{X}}$. Under these transformations, the differential equation (A 1*a*) becomes

$$\xi_{\mathscr{X}} = \frac{m+3+n}{n}\alpha(\xi, \Psi)\xi^2, \tag{A 7a}$$

$$\Psi_{\mathscr{X}} = \alpha(\xi, \Psi)\left[\frac{n-m-3}{n}\Psi\xi + \frac{1}{4}|\Psi|^{-n-1}\Psi - \frac{1}{4}\right], \tag{A 7b}$$

where $\alpha(\xi, \Psi) = \xi^{(mn+n-m-3)/(m+3+n)}|\Psi|^{n-1}\Psi$. Solutions of (A 1*a*) that satisfy the matching conditions (A 1*d*) and (A 1*e*), $\mathscr{U} \to 0$ and $\mathscr{U}^m \sim \mathscr{U}_{\mathscr{X}}/\mathscr{U}^3$ as $X \to -\infty$, now become trajectories that approach the fixed point $(\xi, \Psi) = (0, 1)$. By a change of independent variable in (A 7) to $\zeta = \int_0^{\mathscr{X}} \alpha(\xi(\mathscr{X}'), \Psi(\mathscr{X}'))\,\mathrm{d}\mathscr{X}'$, we can absorb α into the time-like variable and obtain a locally smooth flow in which the fixed point (0, 1) has a stable and a centre manifold (Carr 1981). From (A 7*a*), the centre manifold is unstable, so that in the limit $\mathscr{X} \to -\infty$, a trajectory can therefore approach the fixed point only along the centre manifold. Moreover, the fixed point is therefore a degenerate saddle, so that the centre manifold is, importantly, unique (Sijbrand 1985, theorem 2). This ensures that there is only one orbit into the fixed point.

To solve (A 1), we also have to ensure that the boundary conditions (A 1*b*) and (A 1*c*) are satisfied. In the phase plane, they require that the orbit starts at a point at which $\Psi\xi = \mathscr{U}|\mathscr{U}_{\mathscr{X}}|^{1/n-1}\mathscr{U}_{\mathscr{X}} = \delta/8$, with θ given by the ξ-coordinate of that point through $\theta = \xi^{n/(n+m+3)}$. For small δ, we can make use of the fact that $\Psi \sim 1$ for small ξ, so that $\xi \sim \Psi\xi = \delta/8$, and hence (A 5) holds. More generally, we show that $\Psi\xi$ increases monotonically and without bound as a function of ξ along the centre manifold. Since $\Psi\xi = 0$ at $\xi = 0$, this ensures that there is a single point at which $\Psi\xi = \delta/8$, and also that the ξ-coordinate of that point (and hence the corresponding value of θ) increases monotonically with δ.

From (A 7), the centre manifold satisfies

$$\frac{\mathrm{d}\Psi}{\mathrm{d}\xi} = \frac{n-m-3}{n+m+3}\frac{\Psi}{\xi} - \frac{n}{4(n+m+3)\xi^2}(1-|\Psi|^{-n-1}\Psi), \tag{A 8}$$

and it can be shown that, for small ξ, the centre manifold behaves as $\Psi \sim 1 + 4(n-m-3)\xi/n^2$. We distinguish two cases. If $n-m-3<0$, then the centre manifold is below $\Psi=1$ near $\xi=0$, and, from (A 8), remains below $\Psi=1$ as $(\mathrm{d}\Psi/\mathrm{d}\xi) < 0$ when $\Psi=1$. Similarly, $\mathrm{d}\Psi/\mathrm{d}\xi$ becomes positive as Ψ approaches zero, and Ψ cannot become negative. Consequently, (A 8) implies $\mathrm{d}\Psi/\mathrm{d}\xi > (n-m-3)/(n+m+3)\Psi/\xi$ and hence

$$\frac{\mathrm{d}(\Psi\xi)}{\mathrm{d}\xi} = \xi\frac{\mathrm{d}\Psi}{\mathrm{d}\xi} + \Psi > \frac{2n}{n+m+3}\frac{\Psi\xi}{\xi}. \tag{A 9}$$

Using Gronwall's inequality with a small but finite ξ as a starting point then shows that $\Psi\xi$ is monotonically increasing and grows at least as fast as $\xi^{2n/(n+m+3)}$.

For $n-m-3>0$, the centre manifold is initially above $\Psi=1$ and similarly remains there. In addition, $\mathrm{d}\Psi/\mathrm{d}\xi > 0$ for small ξ. We can then show that $\mathrm{d}\Psi/\mathrm{d}\xi > 0$ everywhere, ensuring that $\mathrm{d}(\Psi\xi)/\mathrm{d}\xi > \Psi > 1$, and again that $\Psi\xi$ is monotonically increasing and unbounded. Differentiating both sides (A 8) and substituting for Ψ/ξ in the resulting expression from (A 8) yields

$$\frac{\mathrm{d}}{\mathrm{d}\xi}\left(\frac{\mathrm{d}\Psi}{\mathrm{d}\xi}\right) = -\left(\frac{2(m+3)}{(n+m+3)\xi} + \frac{n^2}{4(n+m+3)\xi^2\Psi^{n+1}}\right)\frac{\mathrm{d}\Psi}{\mathrm{d}\xi} + \frac{n}{4(n+m+3)\xi^2}(1-\Psi^{-n}). \tag{A 10}$$

As $\Psi > 1$, the last term on the right-hand side is positive. It is then clear that $\mathrm{d}\Psi/\mathrm{d}\xi$ cannot become negative as $\mathrm{d}^2\Psi/\mathrm{d}\xi^2 > 0$ when $\mathrm{d}\Psi/\mathrm{d}\xi = 0$, and the proof is complete.

REFERENCES

Balmforth, N. J. & Craster, R. V. 1999 A consistent thin-layer theory for Bingham plastics. *J. Non-Newtonian Fluid Mech.* **84** (1), 65–81.

Baral, D. R., Hutter, K. & Greve, R. 2001 Asymptotic theories of large-scale motion, temperature distribution in land-based polythermal ice sheets: A critical review and new developments. *Appl. Mech. Rev.* **54** (3), 215–256.

Carr, J. 1981 *Applications of Centre Manifold Theory*. Springer.

Chugunov, V. A. & Wilchinsky, A. V. 1996 Modelling of marine glacier and ice-sheet-ice-shelf transition zone based on asymptotic analysis. *Ann. Glaciol.* **23**, 59–67.

Durand, G., Gagliardini, O., de Fleurian, B., Zwinger, T. & LeMeur, E. 2009 Marine ice sheet dynamics: Hysteresis and neutral equilibrium. *J. Geophys. Res.* **114**, F03009, doi:10.1029/2008JF001170.

Erneux, T. & Davis, S. H. 1993 Nonlinear rupture of free films. *Phys. Fluids* **A5** (5), 1117–1122.

Evatt, G. & Fowler, A. C. 2007 Cauldron subsidence and subglacial floods. *Ann. Glaciol.* **45**, 163–168.

Gagliardini, O., Cohen, D., Raback, P. & Zwinger, T. 2007 Finite-element modeling of subglacial cavities and related friction law. *J. Geophys. Res.* **112** (F2), F02027, doi:10.1029/2006JF000576.

Goldberg, D., Holland, D. M. & Schoof, C. 2009 Grounding line movement and ice shelf buttressing in marine ice sheets. *J. Geophys. Res.* **114**, F04026, doi:10.1029/2008JF001227.

Holland, D. M. & Jenkins, A. 2001 Adaptation of an isopycnic coordinate ocean model for the study of circulation beneath ice shelves. *Mon. Weath. Rev.* **129**, 1905–1927.

Katz, R. F. & Worster, M. G. 2010 Stability of ice-sheet grounding lines. *Proc. R. Soc. Lond.* A **466**, 1597–1620.

Kikuchi, N. & Oden, J. T. 1988 *Contact Problems in Elasticity : A Study of Variational Inequalities and Finite Element Methods*. SIAM.

Lister, J. R. & Kerr, R. C. 1989 The propagation of two-dimensional and axisymmetric viscous gravity currents at a fluid interface. *J. Fluid. Mech.* **203**, 215–249.

Lliboutry, L. 1968 General theory of subglacial cavitation and sliding of temperate glaciers. *J. Glaciol.* **7** (49), 21–58.

MacAyeal, D. R. 1989 Large-scale flow over a viscous basal sediment: theory and application to Ice Stream E, Antarctica. *J. Geophys. Res.* **94** (B4), 4017–4087.

MacAyeal, D. R. & Barcilon, V. 1988 Ice-shelf response to ice-stream discharge fluctuations. I. Unconfined ice tongues. *J. Glaciol.* **34** (116), 121–127.

Muszynski, I. & Birchfield, G. E. 1987 A coupled marine ice-stream–ice-shelf model. *J. Glaciol.* **33** (113), 3–15.

Nowicki, S. M. J. & Wingham, D. J. 2008 Conditions for a steady ice sheet–ice shelf junction. *Earth Planet. Sci. Lett.* **265**, 246–255.

Oron, A., Davis, S. H. & Bankoff, S. G. 1997 Long-scale evolution of thin liquid films. *Rev. Mod. Phys.* **69** (3), 931–977.

Pattyn, F., Huyghe, A., De Brabander, S. & De Smedt, B. 2006 Role of transition zones in marine ice sheet dynamics. *J. Geophys. Res.* **111**, F02004, doi:10.1029/2005JF000394.

Schoof, C. 2005 The effect of cavitation on glacier sliding. *Proc. R. Soc. Lond.* A **461**, 609–627.

Schoof, C. 2006 A variational approach to ice-stream flow. *J. Fluid Mech.* **556**, 227–251.

Schoof, C. 2007*a* Ice sheet grounding line dynamics: steady states, stability and hysteresis. *J. Geophys. Res.* **112**, F03S28, doi:10.1029/2006JF000664.

Schoof, C. 2007*b* Marine ice sheet dynamics. Part 1. The case of rapid sliding. *J. Fluid Mech.* **573**, 27–55.

Schoof, C. & Hindmarsh, R. C. A. 2010 Thin-film flows with wall slip: an asymptotic analysis of higher order glacier flow models. *Q. J. Mech. Appl. Math.* **67** (1), 73–114.

Sijbrand, J. 1985 Properties of center manifolds. *Trans. Am. Math. Soc.* **289** (2), 431–469.

Solomon, S., Qin, D., Manning, M., Marquis, M., Averty, K., Tignor, M., Miller, H. L. & Chen, Z., ed. 2007 *Climate Change 2007: The Scientific Basis*. Cambridge University Press.

van der Veen, C. J. 1983 A note on the equilibrium profile of a free floating ice shelf. *IMAU Rep.* V83-15. State University Utrecht, Utrecht.

Vieli, A. & Payne, A. J. 2005 Assessing the ability of numerical ice sheet models to simulate grounding line migration. *J. Geophys. Res.* **110**, F01003, doi:10.1029/2004JF000202.

Wilchinsky, A. V. & Chugunov, V. A. 2000 Ice stream-ice shelf transition: theoretical analysis of two-dimensional flow. *Ann. Glaciol.* **30**, 153–162.

Wilchinsky, A. V. & Chugunov, V. A. 2001 Modelling ice flow in various glacier zones. *J. Appl. Math. Mech.* **65** (3), 479–493.